


12-2004

Stress Corrosion Cracking Resistance of Martensitic Stainless Steels for Transmutation Applications

Phani P. Gudipati

University of Nevada, Las Vegas

Follow this and additional works at: <https://digitalscholarship.unlv.edu/thesesdissertations>

 Part of the [Mechanical Engineering Commons](#), [Mechanics of Materials Commons](#), [Metallurgy Commons](#), and the [Nuclear Engineering Commons](#)

Repository Citation

Gudipati, Phani P., "Stress Corrosion Cracking Resistance of Martensitic Stainless Steels for Transmutation Applications" (2004). *UNLV Theses, Dissertations, Professional Papers, and Capstones*. 1499.

<http://dx.doi.org/10.34917/3952253>

This Thesis is protected by copyright and/or related rights. It has been brought to you by Digital Scholarship@UNLV with permission from the rights-holder(s). You are free to use this Thesis in any way that is permitted by the copyright and related rights legislation that applies to your use. For other uses you need to obtain permission from the rights-holder(s) directly, unless additional rights are indicated by a Creative Commons license in the record and/or on the work itself.

This Thesis has been accepted for inclusion in UNLV Theses, Dissertations, Professional Papers, and Capstones by an authorized administrator of Digital Scholarship@UNLV. For more information, please contact digitalscholarship@unlv.edu.

**STRESS CORROSION CRACKING RESISTANCE OF MARTENSITIC STAINLESS
STEELS FOR TRANSMUTATION APPLICATIONS**

by

Phani P.Gudipati

**Bachelor of Engineering in Mechanical Engineering
University of Mysore, India
November 2001**

**A thesis submitted in partial fulfillment
of the requirements for the**

**Master of Science Degree in Mechanical Engineering
Department of Mechanical Engineering
Howard R. Hughes College of Engineering**

**Graduate College
University of Nevada, Las Vegas
December 2004**



Thesis Approval
The Graduate College
University of Nevada, Las Vegas

22 November, 2004

The Thesis prepared by

Phani P. Gudipati

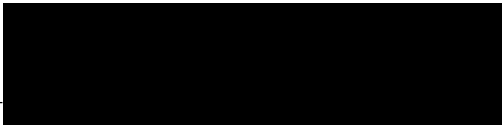
Entitled

Stress Corrosion Cracking of Martensitic Stainless Steels for
Transmutation Applications

is approved in partial fulfillment of the requirements for the degree of

Master of Science in Mechanical Engineering


Examination Committee Chair


Dean of the Graduate College


Examination Committee Member


Examination Committee Member


Graduate College Faculty Representative

ABSTRACT

Stress Corrosion Cracking Resistance of Martensitic Stainless Steels for Transmutation Applications

By

Phani P.Gudipati

Dr. Ajit K.Roy, Examination Committee chair
Associate Professor of Mechanical Engineering
University of Nevada, Las Vegas

The susceptibility of Alloy EP-823 to stress corrosion cracking has been evaluated using smooth and notched cylindrical specimens in neutral and acidic solutions at ambient and elevated temperatures using constant load and slow strain rate testing (SSR) techniques. C-ring and U-bend specimens have also been tested in the acidic solution. The effect of hydrogen on the cracking susceptibility has been evaluated under controlled cathodic potential. While no failures were observed with smooth specimens at constant load, the notched specimens showed failure. The SSR test results indicate that the true failure stress (σ_f), time to failure and ductility parameters were gradually reduced with increasing temperature irrespective of the solution pH. The presence of a notch, however, enhanced the magnitude of σ_f . Neither C-ring nor U-bend specimens showed failure. Optical microscopy of the SSR specimen showed secondary cracking in the 90°C acidic solution. Fractographic evaluation by scanning electron microscopy revealed a combination of ductile (dimples) and brittle (intergranular/transgranular) failures.

TABLE OF CONTENTS

ABSTRACT.....	iii
LIST OF TABLES	vi
LIST OF FIGURES....	vii
ACKNOWLEDGEMENTS	viii
CHAPTER 1 INTRODUCTION.....	1
CHAPTER 2 MATERIAL, TEST SPECIMENS AND ENVIRONMENTS	6
2.1. Test Material.....	6
2.2. Test specimens... ..	8
2.3. Test Environments.....	16
CHAPTER 3 EXPERIMENTAL PROCEDURES	17
3.1. Tensile Testing.....	18
3.2. Constant-Load SCC Testing	19
3.3. Slow-Strain-Rate SCC Testing	21
3.4. SCC Testing under Applied Potential.....	27
3.5. SCC Testing in Autoclave	28
3.6. Optical Microcopy	30
3.7. Scanning Electron Microscopy	31
CHAPTER 4 RESULTS	33
4.1. Constant-Load SCC Tests.....	33
4.2. Slow- Strain-Rate SCC Tests.....	34
4.3. SCC Testing using Self-Loaded Specimens	41
4.4. SCC Testing at Controlled Potential.....	43
4.5. Results of Microscopic Evaluation	44
CHAPTER 5 DISCUSSION	48
5.1. SCC – Constant-Load Testing	48
5.2. SCC – SSR Testing.....	49

5.3. Self-Loaded SCC Testing	50
5.4. SCC Testing under Econt.....	50
5.5. Microscopic Evaluation	50
CHAPTER 6 SUMMARY AND CONCLUSIONS	51
CHAPTER 7 FUTURE WORK	53
APPENDIX.....	54
SLOW-STRAIN-RATE DATA.....	54
BIBLIOGRAPHY.....	68
VITA.....	71

LIST OF TABLES

Table 2.1	Physical and Mechanical Properties of Alloy EP-823 Tested	8
Table 2.2	Chemical Composition of Alloy EP-823 Tested	8
Table 2.3	Chemical Composition of Test Solutions (grams/liter)	16
Table 3.1	Ambient Temperature Tensile Properties of Alloy EP-823	18
Table 4.1	Results of CL SCC Tests using Smooth Specimens.....	34
Table 4.2	Results of CL SCC Tests using Notched Specimens.....	34
Table 4.3	SSR Test Results using Smooth Specimens	37
Table 4.4	SSR Test Results using Notched Specimens	39

LIST OF FIGURES

Figure 1.1	Separation of Fission Products and Actinides.....	2
Figure 2.1	Smooth Tensile Specimen	9
Figure 2.2	Notched Tensile Specimen.....	10
Figure 2.3	Stress Concentration Factors for Grooved Shafts	12
Figure 2.4	C-Ring Specimen	14
Figure 3.1	High-Temperature MTS Unit.....	18
Figure 3.2	Constant-Load Test Setup	20
Figure 3.4	CERT Machines for SSR Testing	22
Figure 3.5	SSR Test Setup.....	23
Figure 3.6	Load Frame Compliance Test	24
Figure 3.8	SSR Test Setup under Econt	28
Figure 3.9	Teflon Fixture for Holding Self-Loaded Specimens.....	29
Figure 3.10	The Autoclave Test Setup	30
Figure 4.1	Comparison of Stress-Strain Diagrams in Neutral Solution	36
Figure 4.2	Comparison of Stress-Strain Diagrams in Acidic Solution.....	36
Figure 4.3	Comparison of Stress-Strain Diagram in Neutral Solution	38
Figure 4.4	Comparison of Stress-Strain Diagram in Acidic Solution	38
Figure 4.5	Effect of pH, Temperature and Specimen Geometry on σ_f	39
Figure 4.6	Effect of pH, Temperature and Specimen Geometry on TTF.....	40
Figure 4.7	Effect of pH, Temperature and Specimen Geometry on %El	40
Figure 4.8	Effect of pH, Temperature and Specimen Geometry on %RA	41
Figure 4.9	Comparison of C-Ring Specimen's appearance.....	42
Figure 4.10	Acidic Environment, Ambient Temperature, Econt= -1000 mV	43
Figure 4.11	Microstructure of Q & T Alloy EP-823, Etched (Fry's Reagent), 10X	44
Figure 4.12	Secondary Cracks, 10X	45
Figure 4.13	Ductile and Brittle Failures in Tensile Specimen at Ambient Temperature in Neutral Solution, 150X.....	46
Figure 4.14	Ductile and Brittle Failures in Tensile Specimen in 90°C Neutral Solution, 150X.....	46
Figure 4.15	Ductile and Brittle Failures in Tensile Specimen at Ambient Temperature in Acidic Solution, 150X.....	47

ACKNOWLEDGEMENTS

I would like to express the deepest appreciation to my committee chair, Principal Investigator in this Project, Dr. Ajit K. Roy. It was my privilege to work with him who continually and convincingly conveyed a spirit of adventure in regard to research and an excitement in learning.

I would like to thank Dr. Anthony Hechanova, Dr. Brendan J O'Toole and Dr. Jacimaria Batista for their direct and indirect contribution throughout this investigation. Special thanks to my colleagues who helped me in many ways.

Words alone cannot express the thanks I owe to Mr. Mohan Rao and Mrs. Annapurna, my father and mother, for their persistence encouragement, sacrifices, support and boundless confidence in me.

Finally I would like to thank the U.S. Department of Energy for financial support of this project.

CHAPTER 1

INTRODUCTION

Generation of energy based on nuclear power source appears to be the most viable method in view of its cleanliness and cost-effectiveness. However, a major problem associated with power generation using nuclear source is the disposal of nuclear wastes.^[1] These wastes can be generated either in the form of spent nuclear fuel (SNF) discharged from commercial reactors or in the form of defense high-level waste (HLW).

Disposal of nuclear wastes using the present day technology has been by burying them underground in a deep geological repository for isolation from the public and the environment.^[2] The Yucca Mountain site near Las Vegas, Nevada has recently been proposed to be the nation's geologic repository^[3] to contain approximately 70,000 metric tons of the SNF and HLW for a prolonged duration.^[4] Such a long disposal period is intended to ensure a gradual reduction in radioactivity of these wastes by natural decay so that the ground water underneath this repository may not get contaminated in course of time. However, with time, more radioactive wastes will be generated from the existing nuclear power plants, thus, requiring their disposal in repositories to be built in future.

In order to circumvent the problems associated with the future disposal of nuclear waste, the United States Department of Energy (DOE) has initiated an extensive effort to develop a method of reduction in radioactivity of HLW and SNF prior to their disposal in

a potential repository. This method, known as transmutation, is based on the reduction in radioactivity of HLW/SNF by bombarding them with neutrons generated either from an accelerator or a reactor thus, transforming the highly radioactive waste into a less radioactive material, as shown in Figure 1.1.

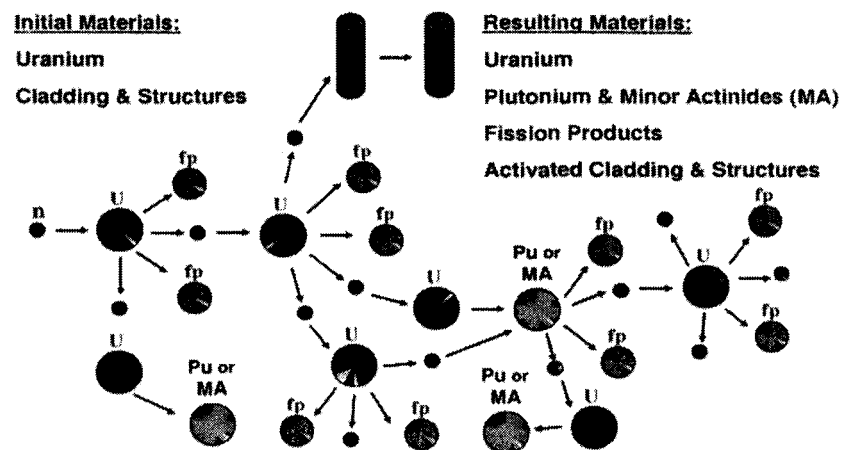


Figure 1.1 Separation of Fission Products and Actinides.

(Courtesy U.S. Department of Energy)

These neutrons are generated by impinging protons from an accelerator onto a target material such as tungsten or molten lead-bismuth-eutectic (LBE) that can also act as a coolant during the transmutation process. The molten LBE will be contained in a sub-system structure made of a suitable material such as a martensitic stainless steel. A flowchart illustrating a comparison of different SNF/HLW disposal processes is shown in Figure 1.2.

Transmutation is currently being practiced in Europe using conventional reprocessing, in particular, the United Kingdom and France. During this past decade, these countries have made significant progress in partitioning and transmuting the long-lived actinides from SNF. The U.S. Department of Energy and its national laboratories have begun to explore the transmutation concept as an alternative waste management strategy. It is anticipated that the transmutation of SNF/HLW may enable the disposal of substantially less radioactive waste inside the proposed geologic repository at the Yucca Mountain site for shorter durations.

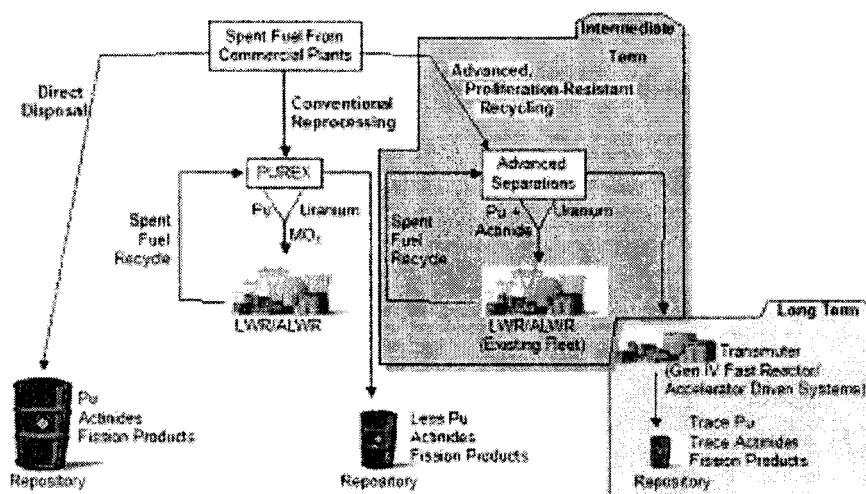


Figure 1.2 Spent Nuclear Fuel Management Approach

(Courtesy U.S. Department of Energy)

During the transmutation process, hydrogen and helium can be generated, which may cause degradation to the target structural material. Further, since this structural material will be subjected to high stresses due to the bombardment of protons onto the target, the structural material may suffer environment induced degradation such as liquid

metal embrittlement, stress corrosion cracking (SCC) and hydrogen embrittlement (HE).^[5-6] However, the mechanism of cracking in the presence of molten LBE is somewhat different from that in the presence of aqueous environments.

The anticipated cracking in the molten LBE may usually fall under the category of liquid-metal-embrittlement (LME) that involves the reduction in cohesive strength of the structural metal surface due to its interaction with the molten metal. On the other hand, degradations such as SCC and HE are related to electrochemical mechanisms involving anodic and cathodic reactions, while exposed to aggressive aqueous environments in the stressed condition.

In view of this rationale, a research program was undertaken to evaluate the cracking behavior of martensitic Alloy EP-823 in the presence of both molten LBE and aqueous solutions. Testing using self-loaded specimens was planned to be performed at the Los Alamos National Laboratory (LANL) in the molten LBE environment. However, due to some facility scheduling and availability problems, this testing could not be accommodated at the LANL. Due to this shortcoming, it has now been proposed to develop a LBE testing facility at UNLV in the very near future.

In the mean time, extensive corrosion studies have been performed at the UNLV's Material Performance Laboratory (MPL) involving Alloy EP-823 in aqueous environments of different pH values at ambient and elevated temperatures. While a direct comparison of the cracking susceptibility of this alloy cannot be made in molten metal and aqueous environments, some comparisons of the surface film could however, be made if the LBE corrosion data were available from LANL.

This thesis presents the results of SCC and HE testing of Alloy EP-823 in neutral and acidic solutions at ambient and elevated temperatures. State-of-the art experimental techniques such as constant load, slow strain rate and self-loaded devices such as C-ring and U-bend have been used to evaluate the cracking susceptibility. In addition, a limited number of testing was performed under controlled cathodic potential to study the effect of hydrogen on cracking behavior of this alloy. Further, metallographic and fractographic evaluations were performed by using optical microscopy and scanning electron microscopy, respectively.

Relevant literature data on Alloy EP-823, environments tested, different experimental techniques used, analysis and discussion of resultant data on SCC/HE, microscopic evaluation, and significant conclusions derived from this investigation are included in subsequent sections.

CHAPTER 2

MATERIAL, TEST SPECIMENS AND ENVIRONMENTS

2.1. Test Material

Martensitic stainless steels are currently finding extensive applications in nuclear reactors as substitutes for austenitic steels.^[7] They are basically alloys of carbon (C) and chromium (Cr) having body-centered cubic (BCC) or body-centered tetragonal (BCT) martensitic crystal structures in the hardened state. They are ferromagnetic, and hardenable by heat-treatments. Martensitic stainless steels are usually preferred for their relatively high strength, moderate corrosion resistance and optimum fatigue properties, following suitable thermal treatments.^[8]

The Cr content of martensitic stainless steel normally ranges between 9 to 18 wt%, and their C content can be as high as 1.2 wt%. The composition of Cr and C are balanced to ensure a martensitic structure after hardening. Molybdenum (Mo) and nickel (Ni) can also be added to improve the mechanical properties or the corrosion resistance. When higher Cr levels are used to improve corrosion resistance due to the formation of chromium oxide (Cr_2O_3), the presence of Ni can also help in maintaining the desired microstructure and preventing the formation of excessive free-ferrite.^[9]

Since the as-hardened martensitic structure is quite brittle, this material is typically reheated at lower temperatures to relieve the internal stresses within the microstructure or

reheated to slightly higher temperatures to soften (temper) the material to intermediate hardness levels. Alloy EP-823, a martensitic stainless steel containing iron-nickel-chromium-molybdenum (Fe-Ni-Cr-Mo), has been extensively used in Russia as a target structural material in the transmutation systems. This type of material has also been used in the United States as internal components in experimental liquid metal fast breeder reactors (LMFBR) due to its moderate corrosion resistance, optimum strength, ease of manufacturing and relatively lower cost.^[10] This alloy possesses significant resistance to swelling during high neutron exposure at temperatures up to 420°C and a low rate of irradiation creep.^[11-12] This alloy has also been reported to retain its high strength and ductility at elevated temperatures in irradiated conditions.^[13] The physical and mechanical properties of Alloy EP-823 are shown in Table 2.1.^[14]

Experimental heats of Alloy EP-823 were melted at the Timken Research Laboratory, Ohio, by a vacuum-induction-melting practice followed by processes that included forging and hot rolling. These hot rolled products were subsequently cold rolled to produce round bars of different sizes. These cold-rolled bars were initially austenitized at 1010°C followed by oil-quenching. Hard but brittle martensitic microstructures were developed in these bars due to austenitizing and quenching. Therefore, tempering operations were performed at 621°C to produce fine-grained and fully-tempered martensitic microstructures without the formation of any retained austenite, thus producing appreciable ductility. The chemical composition of Alloy EP-823 is shown in Table 2.2.

Table 2.1 Physical and Mechanical Properties of Alloy EP-823 Tested

Property	Alloy EP-823
Thermal Conductivity W/m*K	Not Available
Modulus of Elasticity, Gpa (10^6 psi)	207
Poisson's ratio	0.29
Coefficient of Thermal Expansion ($^{\circ}\text{C}$) $\ast 10^{-6}$	Not Available
Yield Strength (ksi)	111

Table 2.2 Chemical Composition of Alloy EP-823 Tested

Alloy EP-823/Heat No. 2056	Elements	Wt %
	C	0.14
	Mn	0.56
	P	0.013
	S	0.005
	Si	1.11
	Cr	11.68
	Ni	0.66
	Mo	0.73
	Cu	0.002
	V	0.30
	W	0.62
	Cb	0.22
	B	0.009
	Ce	0.05

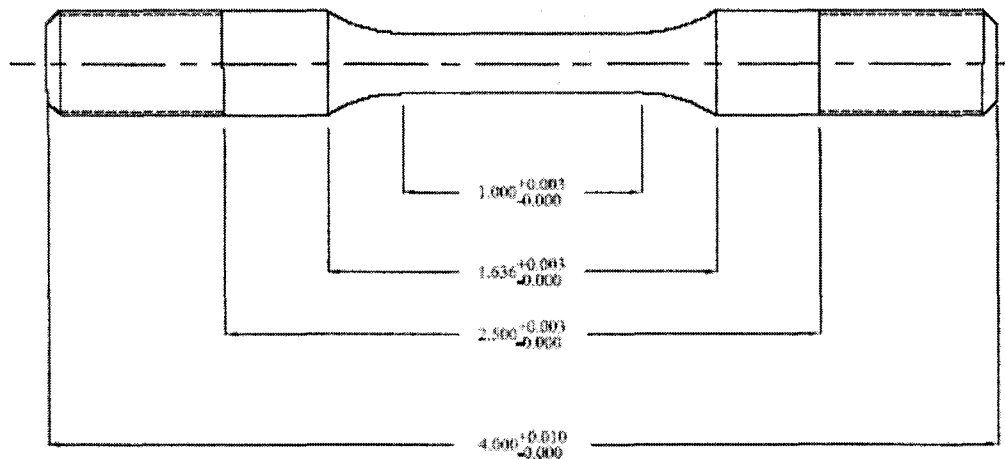
2.2. Test specimens

Cylindrical smooth specimens having 4-inch total length, 1-inch gage length and 0.25-inch gage diameter were machined from the heat-treated round bars in the

longitudinal rolling direction. Some of these cylindrical tensile specimens were modified by machining a V-shaped notch having an angle of 60° and a 0.05-inch depth around the diameter (0.156-inch) at the center of the gage section. The configurations of both smooth and notched cylindrical specimens are shown in Figures 2.1 and 2.2, respectively.

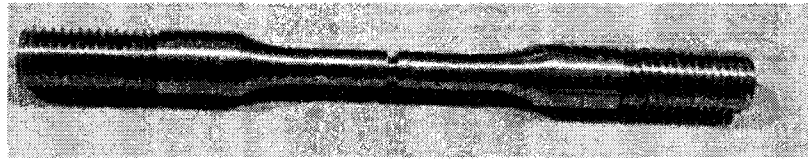


(a) Pictorial View

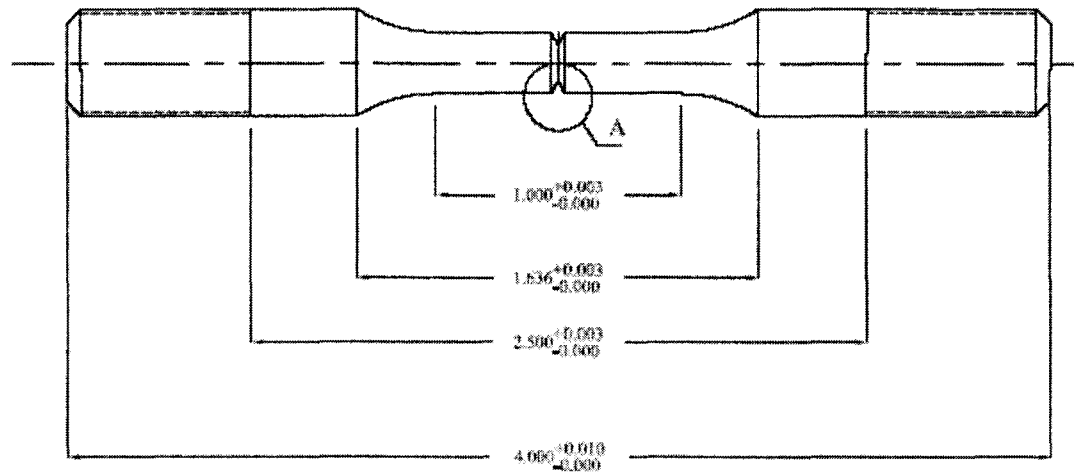


(b) Dimensions

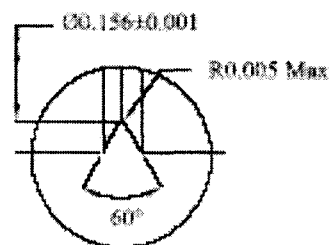
Figure 2.1 Smooth Tensile Specimen



(a) Pictorial View



View A



(b) Dimensions

Figure 2.2 Notched Tensile Specimen

The stress concentration factor (K_t) corresponding to the presence of the notch was estimated using the dimension of the notched specimen and the plot ^[15] shown in Figure

The stress concentration factor (K_t) corresponding to the presence of the notch was estimated using the dimension of the notched specimen and the plot ^[15] shown in Figure 2.3. Related calculations to arrive at this value are shown below. The magnitude of K_t was found to be approximately 1.45 using both D/d and r/d ratios, as shown in the figure.

$$\frac{D}{d} = \frac{0.250 \text{ in}}{0.156 \text{ in}} \quad (\text{Equation 2.1})$$
$$\frac{D}{d} = 1.60$$

$$\frac{r}{d} = \frac{0.05 \text{ in}}{0.156 \text{ in}} \quad (\text{Equation 2.2})$$
$$\frac{r}{d} = 0.32$$

Where,

D = gage diameter,

d = notch diameter

r = radius of curvature at the root of the notch

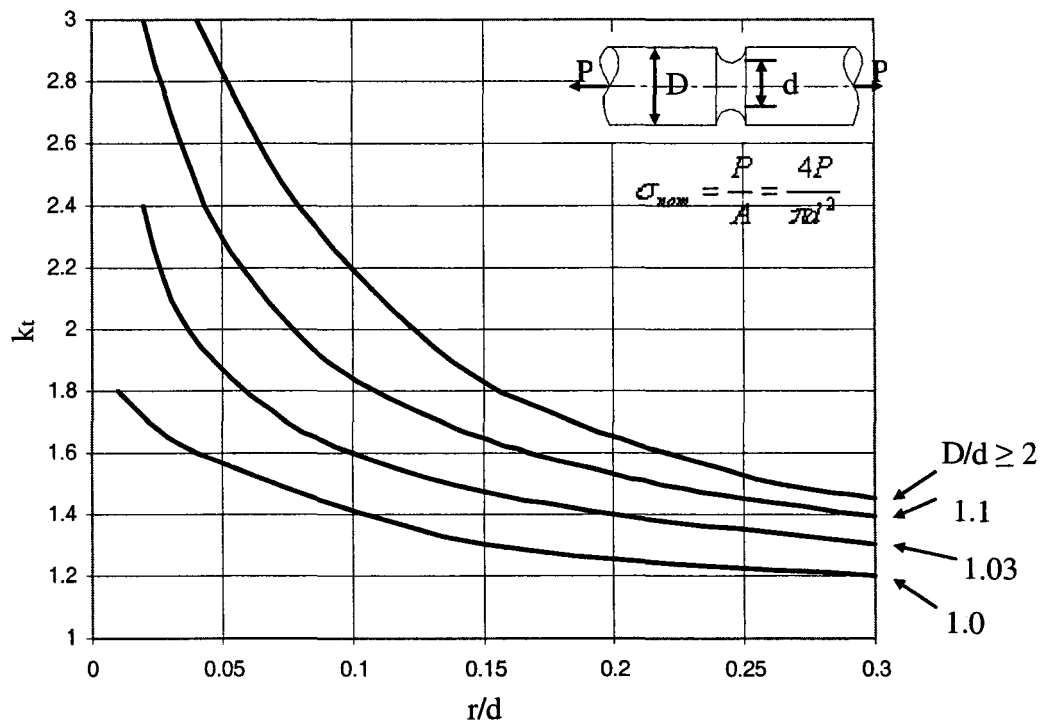


Figure 2.3 Stress Concentration Factors for Grooved Shafts

(Source: Modified from Robert C. Juvinall et al., *Fundamentals of Machine Component Design*, John Wiley & Sons, Inc., 2nd edition, 1991)

In addition to the cylindrical specimens, self-loaded specimens such as C-ring and U-bend were used in this investigation, as illustrated in Figures 2.4 and 2.5, respectively. The C-ring is a versatile and economic type of specimen for quantitatively determining the susceptibility of a material to SCC of all types of alloys in a wide variety of product forms. It is particularly suitable for making transverse tests of tubing and rod and for making short-transverse tests of various products. The U-bend specimen is generally a rectangular strip which is bent 180° around a predetermined radius and maintained in this constant strain condition during the stress corrosion test. Sizes for C-rings may be varied over a wide range, but C-rings with an outside diameter less than about 16 mm are not

recommended because of increased difficulties in machining and decreased precision in stressing.^[16-17] The equation used to determine the applied stress for the C-ring specimen was taken from the ASTM designation G 38^[16] which is shown below.

$$OD_f = OD - \Delta, \text{ and} \quad (\text{Equation 2.3})$$

$$\Delta = f \cdot \pi \cdot D^2 / 4 \cdot E \cdot t \cdot Z$$

Where,

OD = outside diameter of C-ring before stressing, in (or mm),

OD_f = outside diameter of stressed C-ring, in (or mm),

f = desired stress, MPa (or psi) (within the proportional limit),

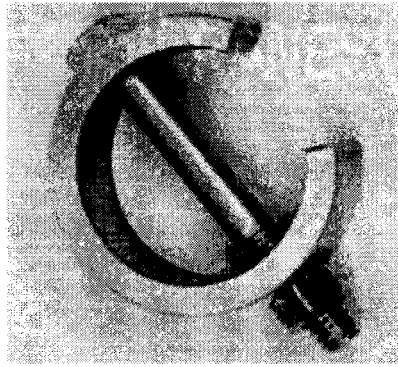
Δ = change in OD giving desired stress, mm (or in.),

D = mean diameter (OD – t), mm (or in.),

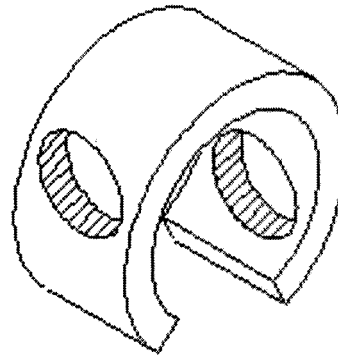
t = wall thickness, mm (or in.),

E = modulus of elasticity, MPa (or psi), and

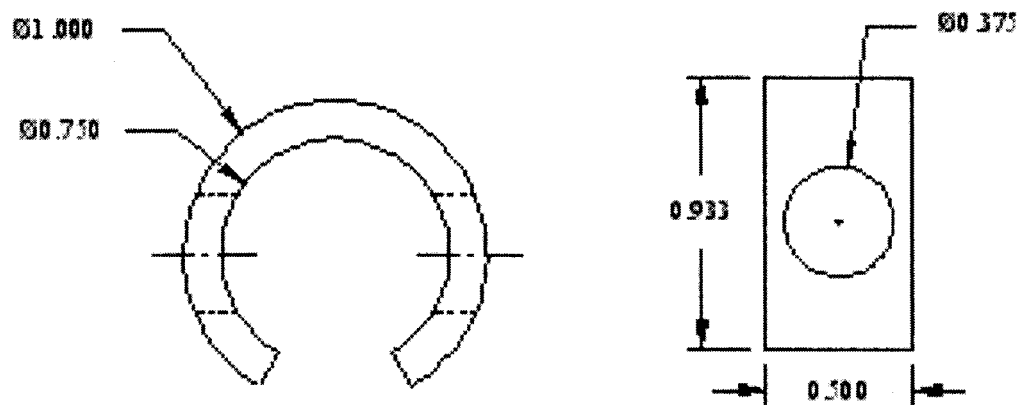
Z = a correction factor for curved beams.



(a) Pictorial View

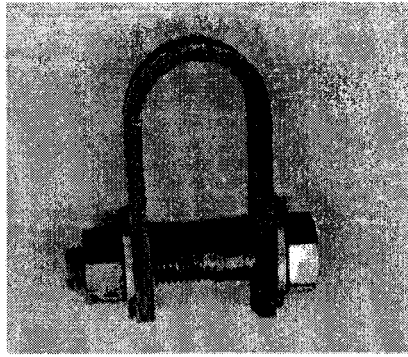


(b) Drawing

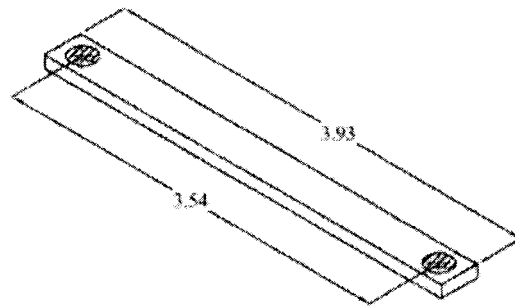


(c) Dimensions

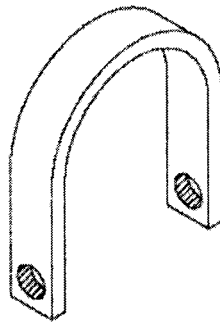
Figure 2.4 C-Ring Specimen



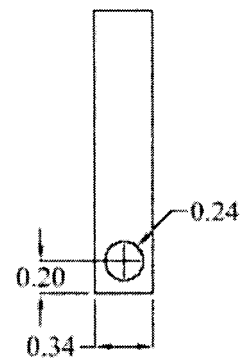
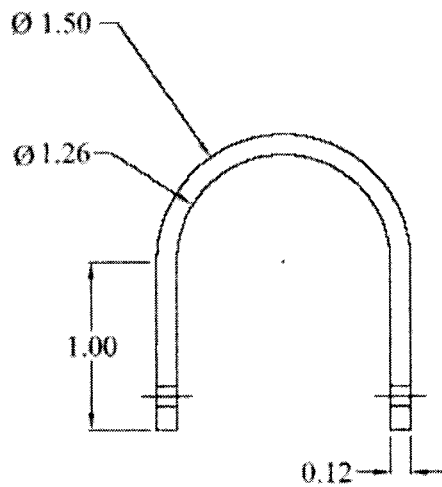
(a) Pictorial View



(b) Drawing- Initial View



(c) Drawing – Final View



(d) Dimensions

Figure 2.5 U-Bend Specimen

2.3. Test Environments

The planned SCC testing using C-ring and U-bend specimens could not be performed at LANL. Therefore, corrosion studies were performed at the MPL. These studies were performed in neutral and acidic aqueous environments at 30, 60 and 90°C. The selection of these environments was based on a rationale that an acidic solution with a pH of approximately 2.0 and slightly above could simulate a very aggressive testing environment to evaluate the cracking susceptibility of Alloy EP-823. Simultaneously, the performance of testing in a neutral solution was aimed to compare the cracking susceptibility of Alloy EP-823 in this environment to that in the acidic solution. The compositions of both test solutions are given in Table 2.3, which were used in the SCC testing involving all types of test specimens.

Table 2.3 Chemical Composition of Test Solutions (grams/liter)

Environment (pH)	CaCl ₂	K ₂ SO ₄	MgSO ₄	NaCl	NaNO ₃	Na ₂ SO ₄
Neutral (6-6.5)	2.769	7.577	4.951	39.973	31.529	56.742
Acidic (2-2.5)	Same as above except for an addition of HCl to attain the desired pH range					

CHAPTER 3

EXPERIMENTAL PROCEDURES

The study of environment-assisted-cracking involves the consideration and evaluation of the inherent compatibility between a material and susceptible environment under conditions of either applied or residual stress. As indicated earlier, Alloy EP-823 has been used as a structural material to contain molten LBE during the transmutation process.^[18] During this process, significant amount of heat, hydrogen, helium and stress may be generated, causing environment-assisted-degradation such as liquid-metal-embrittlement of this structural material.

In view of the above rationale, testing involving self-loaded specimens was planned to be performed at LANL using its LBE loop to evaluate the susceptibility of Alloy EP-823 to liquid metal embrittlement. Unfortunately, this testing could not be accommodated at LANL due to some technical difficulty. Simultaneously, an extensive testing program was initiated involving Alloy EP-823 at UNLV using its Materials Performance Laboratory (MPL), which included the evaluations of the tensile properties, the determination of the susceptibilities to SCC/HE in aqueous environments, and the metallurgical characterization using numerous state-of-the-art experimental techniques. The detailed experimental procedures are described in the following sub-sections.

3.1. Tensile Testing

An axial/torsional servo hydraulic and computer-controlled MTS unit was used to determine the tensile properties of Alloy EP-823 including the yield strength (YS), ultimate tensile strength (UTS) and ductile parameters such as percentage elongation (%El) and percentage reduction in area (%RA) at ambient temperature according to the ASTM Designation E 8.^[19] A model 319.25 MTS equipment used in tensile testing is shown in Figure 3.1. The strain rate used in this testing was 10^{-3} s^{-1} . The room temperature tensile properties are shown in Table 3.1.

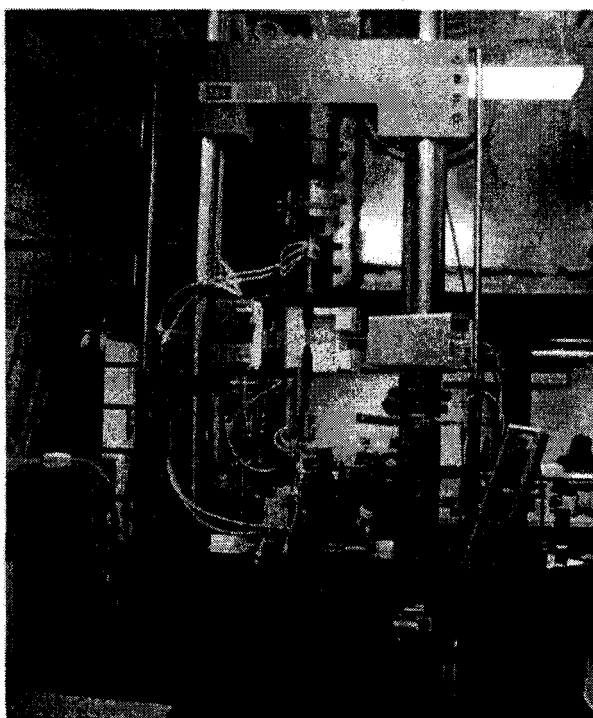


Figure 3.1 High-Temperature MTS Unit

Table 3.1. Ambient Temperature Tensile Properties of Alloy EP-823

Material/Heat No.	Yield Strength (ksi)	%El	%RA	R _C
Alloy EP-823/2056	102.60	21.00	61.00	30.33

3.2. Constant-Load SCC Testing

Calibrated proof rings were used for constant-load (CL) SCC testing. These proof rings were specially designed to meet a National Association of Corrosion Engineers (NACE) standards.^[20] Each individually-calibrated proof ring, made of precision-machined alloy steel by the Cortest Inc., Ohio, was accompanied by a calibration curve showing the load versus deflection of this ring. Test specimens were loaded under a stress state of uniaxial tension. Ring deflection was measured with a 8-9" diameter micrometer, with the supplied dial indicator providing a check. The tensile load on the proof ring was quickly and easily adjusted using a standard wrench on the tension-adjusting screw and lock nut. A thrust bearing distributed the load and prevented seizure. Specimen grips in these proof rings were made of austenitic stainless steel, fully-resistant to the testing environments. The environmental test chamber was secured by O-ring seals that prevented any leakage during testing. The environmental chambers, made of highly corrosion-resistant Hasteloy C-276, were used for testing at elevated temperatures. The experimental setup is shown in Figure 3.2.

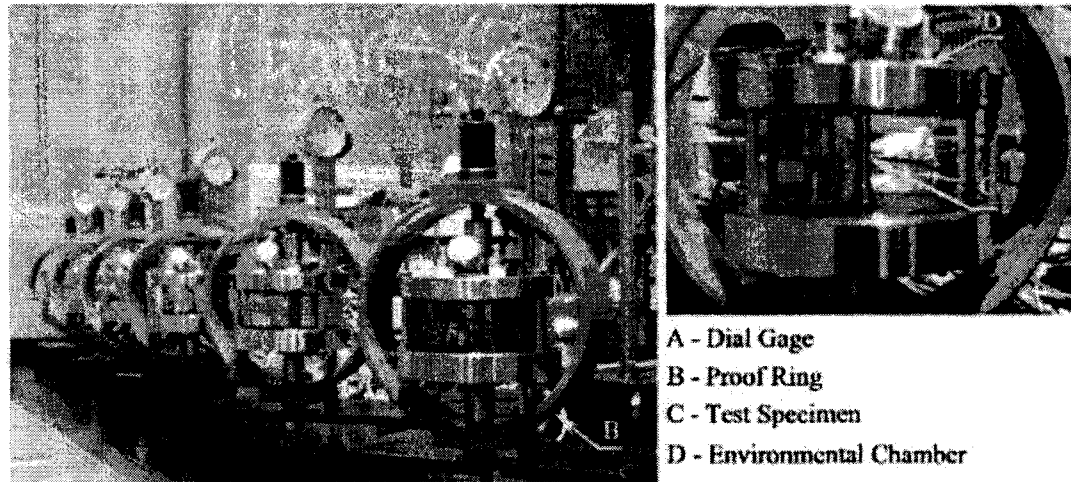


Figure 3.2 Constant-Load Test Setup

The amount of deflection needed to apply the desired load in the CL testing was determined by use of the calibration curve of the proof ring, shown in Figure 3.3. The magnitude of the applied stress was based on the ambient temperature tensile YS of the test material. The specimens were loaded at stress values equivalent to different percentages of the individual material's YS value, and the corresponding time-to-failure (TTF) was recorded. The determination of the SCC tendency using this technique was based on the TTF for the maximum test duration of 30 days. An automatic timer attached to the test specimen recorded the TTF. The cracking susceptibility was expressed in terms of a threshold stress (σ_{th}) below which cracking did not occur during the maximum test duration of 30 days.

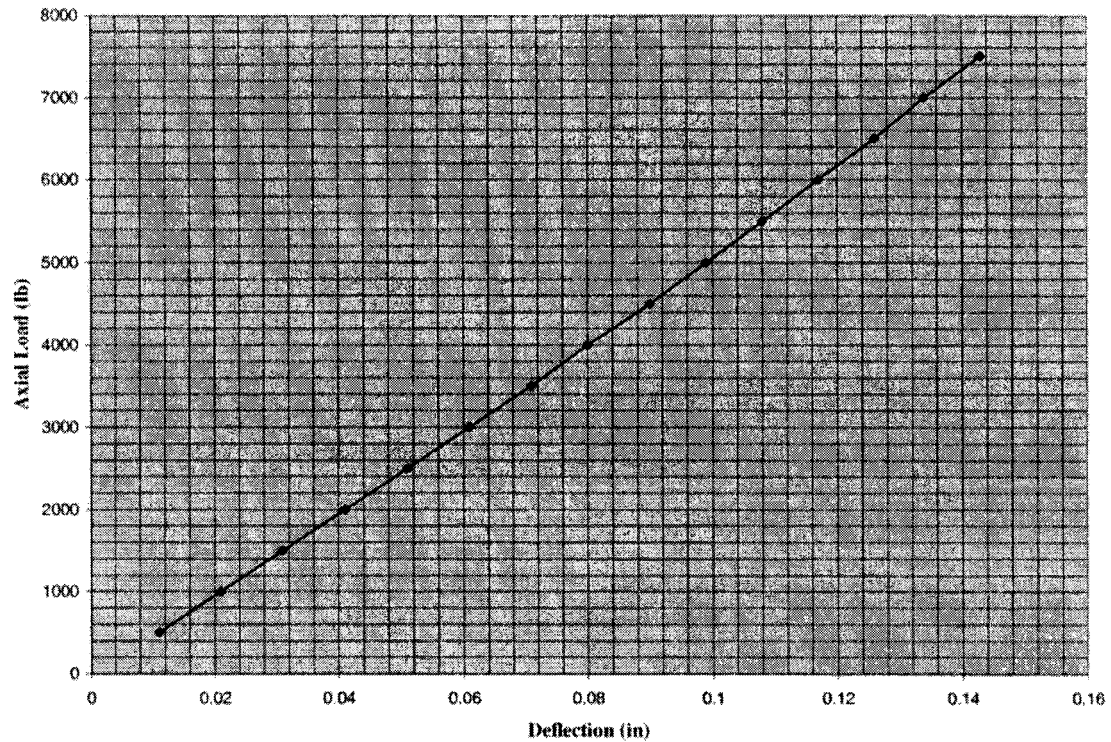


Figure 3.3 A Typical Calibration Curve for a Proof Ring

3.3. Slow-Strain-Rate SCC Testing

SCC testing using the slow-strain-rate (SSR) technique was performed in a specially-designed system known as a constant-extension-rate-testing (CERT) machine, shown in Figure 3.4. This equipment (model 3451) allowed testing to simulate a broad range of load, temperature, pressure, strain-rate and environmental conditions using both mechanical and electrochemical corrosion testing techniques. These machines, designed and manufactured by Cortest Inc., offered accuracy and flexibility in testing the effects of strain rate, providing up to 7500 lbs of load capacity with linear extension rates ranging from 10^{-5} to 10^{-8} in/sec.

To ensure the maximum accuracy in test results, this apparatus was comprised of a heavy-duty load-frame that minimized the variation in system compliance while

maintaining precise axial alignment of the load train. An all-gear drive system provided consistent extension rate. This machine provided the maximum flexibility and working space for test sample configuration, environmental chamber design, and accessibility. An added feature included in this equipment for ease of operation was a quick-hand wheel to apply a preload prior to the operation.

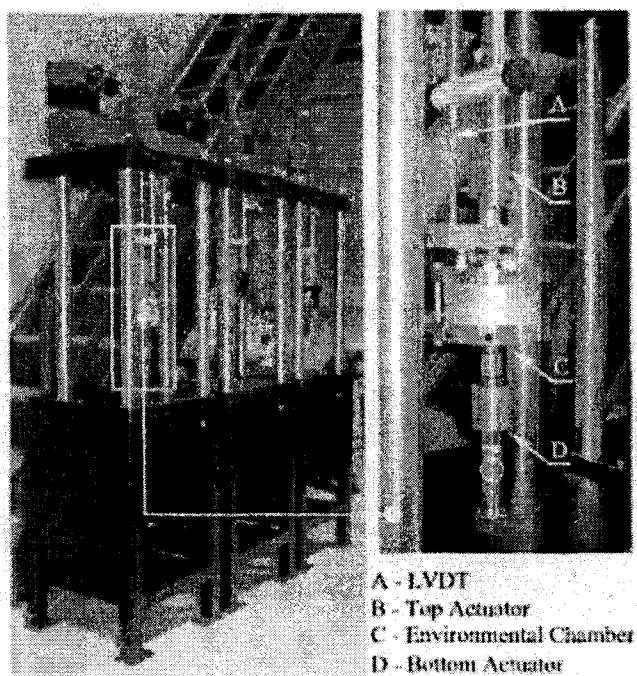


Figure 3.4 CERT Machines for SSR Testing

The SSR test setup used in this study consisted of a top-loaded actuator, a testing chamber, a linear variable differential transducer (LVDT) and a load cell, as shown in Figure 3.5. The top-loaded actuator was intended to pull the specimen at a specified strain rate so that the spilled solution, if any, would not damage the actuator. A heating cartridge was connected to the bottom cover of the environmental chamber for elevated-

temperature testing. A thermocouple was connected on the top cover of this chamber to monitor the inside temperature. The load cell was intended to measure the applied load through an interface with the front panel user interface. The LVDT was used to record the displacement of the gage section during the SSR testing.

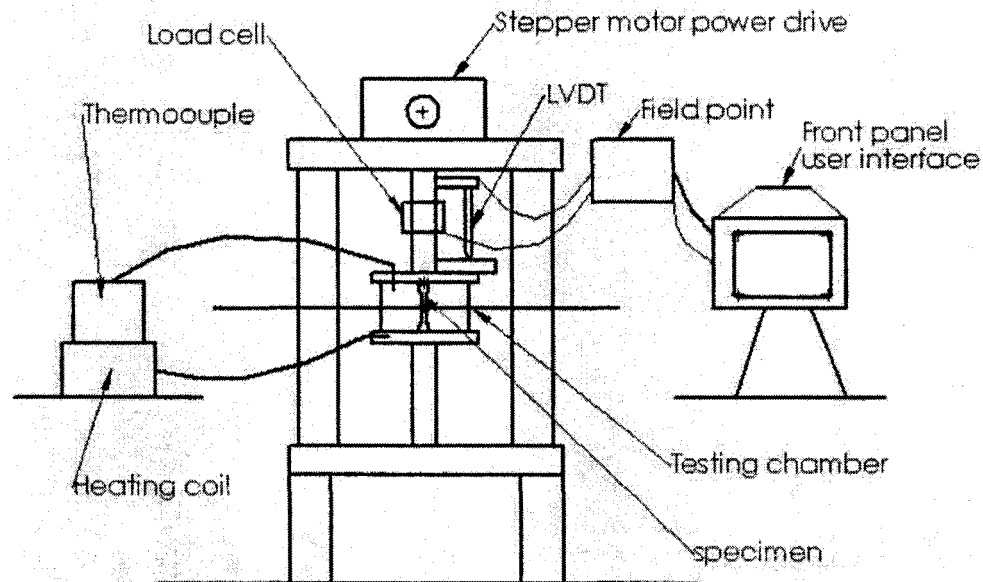


Figure 3.5 SSR Test Setup

Prior to the performance of SCC testing by this technique, the load-frame-compliance factor (LFCF- the deflection in the frame per unit load), was determined by using a ferritic type 430 stainless steel specimen. The generated LFCF data are shown in Figure 3.6. These LFCF values were inputted to a load frame acquisition system prior to the SCC testing.

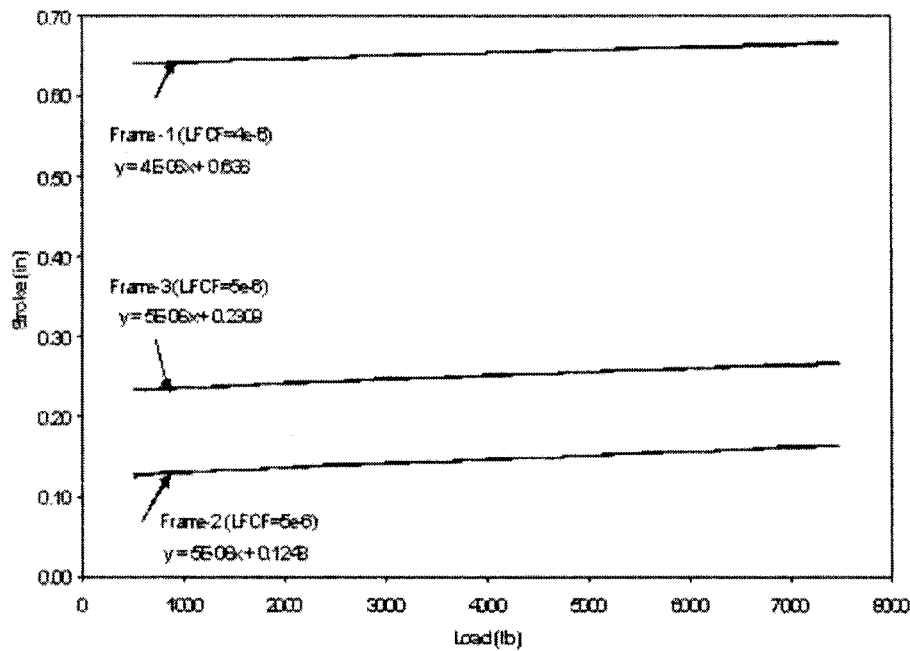


Figure 3.6 Load Frame Compliance Test

A strain rate of $3.3 \times 10^{-6} \text{ s}^{-1}$ was used during the SSR testing. This strain rate was selected based upon prior research work performed at the Lawrence Livermore National Laboratory (LLNL).^[21] It is well known that the SCC phenomenon is based on two significant factors including an applied or a residual stress and a susceptible environment. If the stress is applied at a very fast rate to the test specimen, while it is exposed to the aqueous environment, the resultant failure may not be different from the conventional mechanical deformation produced without an environment. On the other hand, if the strain rate is too slow, the resultant failure may simply be attributed to the corrosive damage due to environmental interaction with the material, thus, causing breakdown of the protective surface film.

In view of the above rationale, the SSR testing at LLNL was initially conducted at strain rates ranging between 10^{-5} and 10^{-7} s^{-1} . Based upon the experimental work at LLNL, it was determined that a strain rate of around 10^{-6} s^{-1} would provide the most effective contributions of both the mechanical and environmental variables to enhance the environment-induced cracking susceptibility using the SSR testing technique. ^[21]

During SCC testing by the SSR method, the specimen was continuously strained in tension until fracture, in contrast to the more conventional SCC test conducted under a sustained loading condition. The application of a slow dynamic straining during the SSR testing to the specimen caused failure that probably might not occur under a constant load or might have taken a prohibitively longer duration to initiate cracks in producing failures in the tested specimens.

Load versus displacement, and stress versus strain curves were plotted during these tests. Dimensions (length and diameter) of the test specimens were measured before and after testing. The cracking tendency in the SSR tests was characterized by the TTF, and a number of ductility parameters including the %El and %RA. Further, the maximum stress (σ_m) and the true failure stress (σ_f) obtained from the stress-strain diagram and the final specimen dimensions were taken into consideration. The magnitudes of %El, %RA, σ_m and σ_f were calculated using the following equations:

$$\% \text{ El} = \left(\frac{L_f - L_o}{L_o} \right) \times 100 ; L_f > L_o \quad (\text{Equation 3.1})$$

$$\% \text{ RA} = \left(\frac{A_o - A_f}{A_o} \right) \times 100 ; A_o > A_f \quad (\text{Equation 3.2})$$

$$\sigma_f = \frac{P_f}{A_f} \quad (\text{Equation 3.3})$$

$$\sigma_m = \frac{P_m}{A_m} \quad (\text{Equation 3.4})$$

$$A_o = \frac{\pi \times D_o^2}{4} \quad (\text{Equation 3.5})$$

$$A_f = \frac{\pi \times D_f^2}{4} \quad (\text{Equation 3.6})$$

Where,

A_o = Initial cross sectional area

A_m = Cross sectional area at maximum load

A_f = Final cross sectional area at failure

P_m = Ultimate tensile load

P_f = Failure load

L_o = Initial length

L_f = Final length

D_o = Initial diameter

D_f = Final diameter

3.4. SCC Testing under Applied Potential

A limited number of SCC tests were performed in the acidic solution using the SSR technique at controlled cathodic potential (E_{cont}) to study the effect of hydrogen on the cracking susceptibility of Alloy EP-823. The magnitude of E_{cont} was based on the corrosion potential (E_{corr}) of this material performed in a similar environment by a previous investigator.^[22] The desired electro-chemical potential was applied to the cylindrical specimen by spot-welding a stainless steel wire at the shoulder of the specimen, as illustrated in Figure 3.7.^[21, 23-25] The experimental setup for cathodic charging using the SSR testing technique is shown in Figure 3.8.

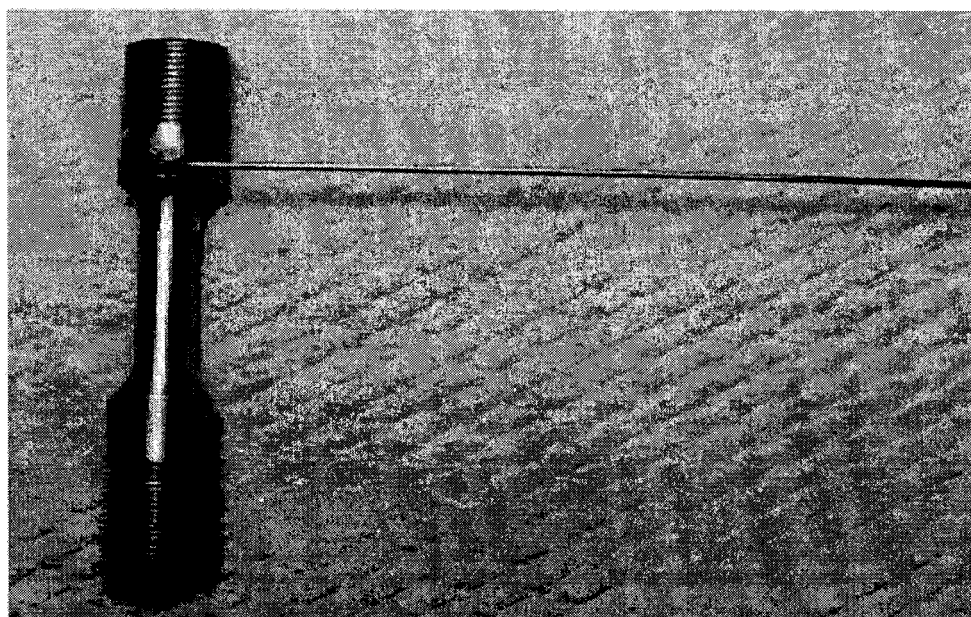


Figure 3.7 Spot-Welded Tensile Specimen

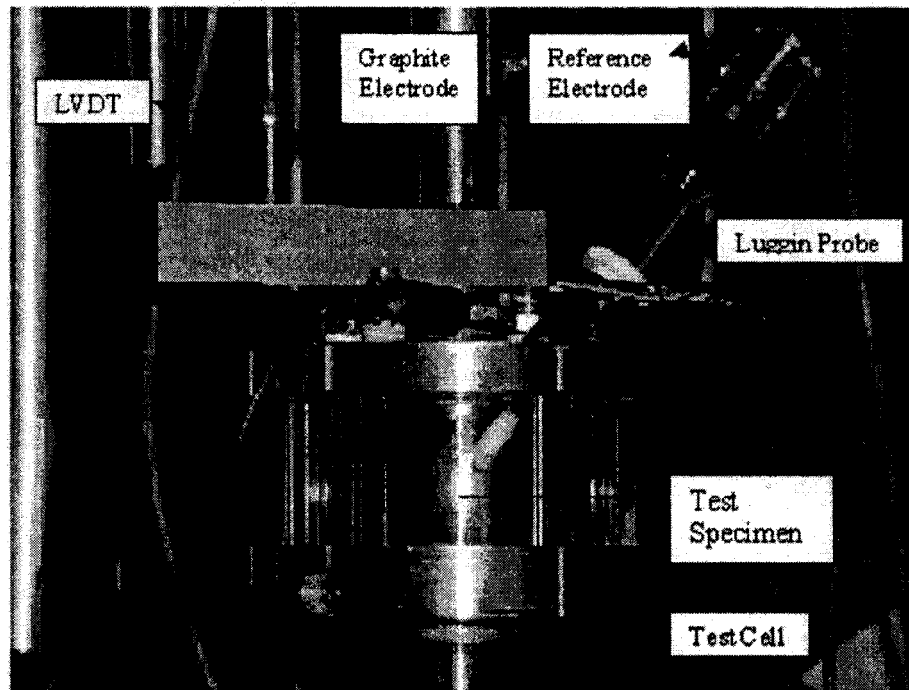


Figure 3.8 SSR Test Setup under Econt

3.5. SCC Testing in Autoclave

As indicated earlier, the primary goal of this research project was to evaluate the environment-induced-degradation in target structural material in the presence of molten LBE. Since, the SCC testing under a controlled-loading condition such as constant load or SSR is difficult to accomplish in an environment containing molten metals, it was decided that the evaluation of cracking using target structural material could better be accomplished by using self-loaded specimens such as C-ring and U-bend.

Since SCC testing in the molten LBE environment using C-ring and U-bend specimens could not be accomplished at the LANL due to the unavailability of their LBE loop facility, testing was planned to be performed at the MPL in aqueous environments contained in an autoclave at temperatures at and above 100°C using similar types of specimens.

A Teflon sample holder was fabricated to place the self-loaded specimens for immersion in the aqueous solutions contained inside the autoclave. The selection of Teflon as the holder material was based on the anticipated testing temperature so that it does not melt under the operating conditions. Temperatures in increments of 50°C were planned for SCC testing using C-ring and U-bend specimens. However, experimental difficulties were experienced at temperatures above 100°C due to the development of vapor pressure at this temperature. Ideally, the gasket for this type of testing was designed to hold temperatures up to 300°C even in the presence of an aqueous environment. In view of this problem, all autoclave tests involving self-loaded specimens were performed at 100°C only. The sample holder and the autoclave test setup are shown in Figures 3.9 and 3.10, respectively.

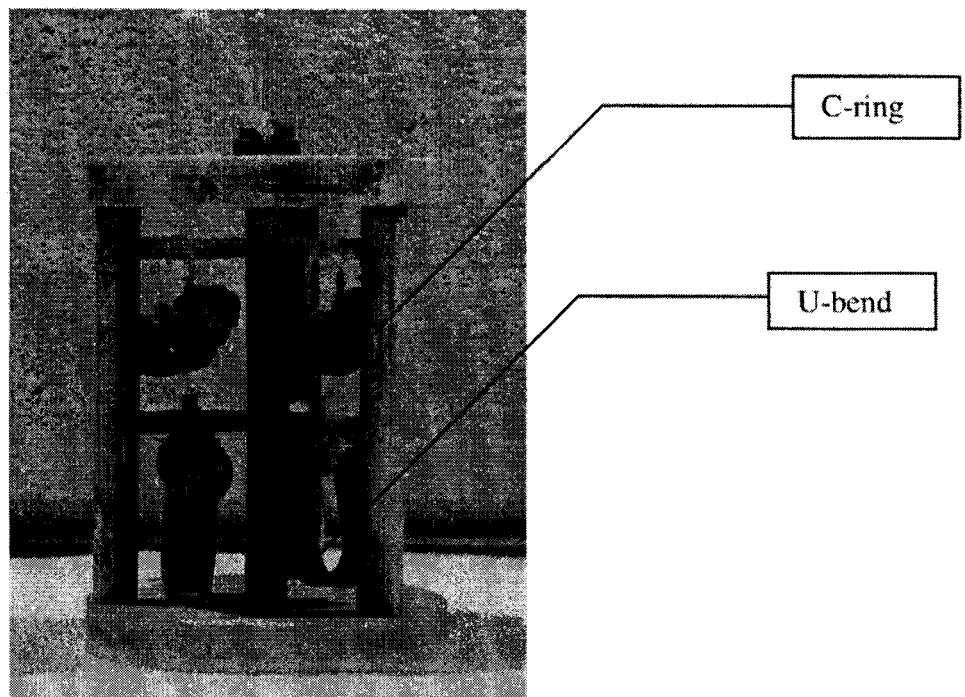


Figure 3.9 Teflon Fixture for Holding Self-Loaded Specimens

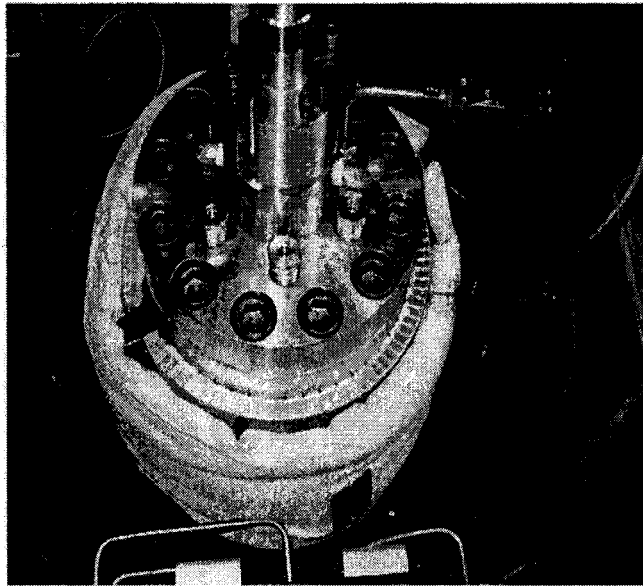


Figure 3.10 The Autoclave Test Setup

3.6. Optical Microscopy

Characterization of metallurgical microstructures of engineering materials by optical microscopy is of great importance. This metallographic technique enables the characterization of phases present, their distributions within grains and their sizes which depend on the typical composition and thermal treatments performed on a material of interest. The principle of an optical microscope is based on the impingement of a light source perpendicular to the test specimen. The light rays pass through the system of condensing lenses and shutters, up to the half-penetrating mirror. This brings the light rays through the objective to the surface of the specimen. Light rays reflected off the surface of the sample then return to the objective, where they are gathered and focused to form the primary image. This image is then projected to the magnifying system of the eyepiece. The contrast observed under the microscope results from either an inherent

difference in intensity or wavelength of the light absorption characteristics of the phases present. It may also be induced by preferential staining or attack of the surface by etching with a chemical reagent.

The tested specimens were sectioned and mounted by standard metallographic technique, followed by polishing and etching to reveal their microstructures including the grain boundaries. The polished and etched specimens were rinsed in deionized water, and dried with acetone and alcohol prior to their evaluation by a Leica microscope (model # 4001) having a magnification of 1000X. The presence of secondary cracks, if any, along the gage section of the failed specimen was also determined by this technique.

3.7. Scanning Electron Microscopy

The extent and morphology of failure in the tested specimens were determined by SEM. Failure analyses of metals and alloys involve identification of the types of the failure. Failure can occur by one or more of several mechanisms, including surface damage, such as corrosion or wear, elastic or plastic deformation and fracture. Failures can be classified as ductile or brittle. Dimpled microstructure is a characteristic of ductile failure. Brittle failure can be of two types, intergranular and transgranular. An intergranular brittle failure is characterized by crack propagation along the grain boundaries while a transgranular failure is characterized by crack propagation across the grains. The morphology of failure in the tested specimen was determined by scanning electron microscopy (SEM). A Jeol SEM (model# 2605) was used to evaluate the fractography of all tested specimen. Energy Dispersive Spectroscopy (EDS), interfaced

with this SEM, was also used for elemental analysis in the vicinity of the resultant failures.

CHAPTER 4

RESULTS

4.1. Constant-Load SCC Tests

The results of SCC testing using smooth cylindrical specimens at constant load in the 90°C neutral and acidic solutions are shown in Table 4.1. These results indicate that no failures were observed with Alloy EP-823 at an applied stress (σ_a) corresponding to 95% of the material's room-temperature yield strength value, irrespective of the test solution. Usually, this type of testing is performed for a maximum duration of 30 days to determine the threshold stress (σ_{th}) below which no failure could occur in an environment of interest. Since no failure was observed at a σ_a value of 0.95YS, it can be construed that the magnitude of σ_{th} for Alloy EP-823 could lie somewhere in between 95 and 100% of the material's YS value.

With respect to the SCC susceptibility of Alloy EP-823 using notched specimens, the results, shown in Table 4.2, clearly indicate that no failures were observed in a 90°C acidic solution when loaded at applied stresses equivalent to 45 and 50% of its YS value. Based on this data, it can be concluded that the magnitude of σ_{th} may lie at around 0.50YS of Alloy EP-823, which is substantially lower compared to that obtained using the smooth specimen. This reduction of σ_{th} value in the notch specimen may be attributed to the stress concentration effect.

Table 4.1 Results of CL SCC Tests using Smooth Specimens

Environment	Temperature (°C)	Applied Stress (ksi)		TTF
		%YS	Stress (ksi)	
Neutral (pH = 6.0 – 6.5)	30	95	105.45	NF
	60	95	105.45	
	90	95	105.45	
Acidic (pH = 2.0 – 2.2)	30	95	105.45	NF
	60	95	105.45	
	90	95	105.45	

TTF : Time To Failure

NF : No Failure

Table 4.2 Results of CL SCC Tests using Notched Specimens

Environment	Temperature	Applied Stress		TTF
		%YS	Stress (ksi)	
Acidic	90°C	45	49.95	NF
		50	55.50	

NF: No Failure

4.2. Slow- Strain-Rate SCC Tests

A comparison of the stress-strain diagrams using smooth cylindrical specimens, obtained in SSR testing incorporating neutral and acidic solutions at different temperatures, are shown in Figures 4.1 and 4.2, respectively. An evaluation of these

figures reveals that the magnitude of strain was gradually reduced with increasing temperature, irrespective of the testing environment. The data shown in these two figures are reproduced in Table 4.3, showing the effect of temperature and pH on the true failure stress (σ_f), the time to failure (TTF) and the ductility parameters such as %El and %RA. These parameters are conventionally used to characterize the cracking susceptibility of a material of interest when tested by the SSR technique.

An examination of Table 4.3 reveals that the magnitude of σ_f , TTF, %El and %RA was gradually reduced with increasing temperature, showing more pronounced effect in the acidic environment. The stress-strain diagrams obtained in neutral and acidic solutions using notched specimens are illustrated in Figures 4.3 and 4.4, respectively, once again showing reduced strains at higher testing temperatures. The magnitude of σ_f , TTF, %El and %RA determined from these plots are given in Table 4.4, showing a similar trend on the effect of temperature and pH on these parameters, as observed earlier with the smooth specimens.

The results of SSR testing using smooth and notched cylindrical specimens shown in Tables 4.3 and 4.4, are graphically reproduced in Figures 4.5 through 4.8 showing the effect of pH, temperature and specimen geometry on σ_f , TTF, %El, and %RA. Examination of these figures clearly indicates that all these parameters were reduced in either environment at elevated temperatures, showing more pronounced effect in the acidic solution. The presence of a notch significantly reduced TTF, %El, and %RA. However, the magnitude of σ_f was increased with the notched specimens due to the relatively smaller cross-sectional area at the root of the notch that also produced a large mechanical constraint in the vicinity of the notch.

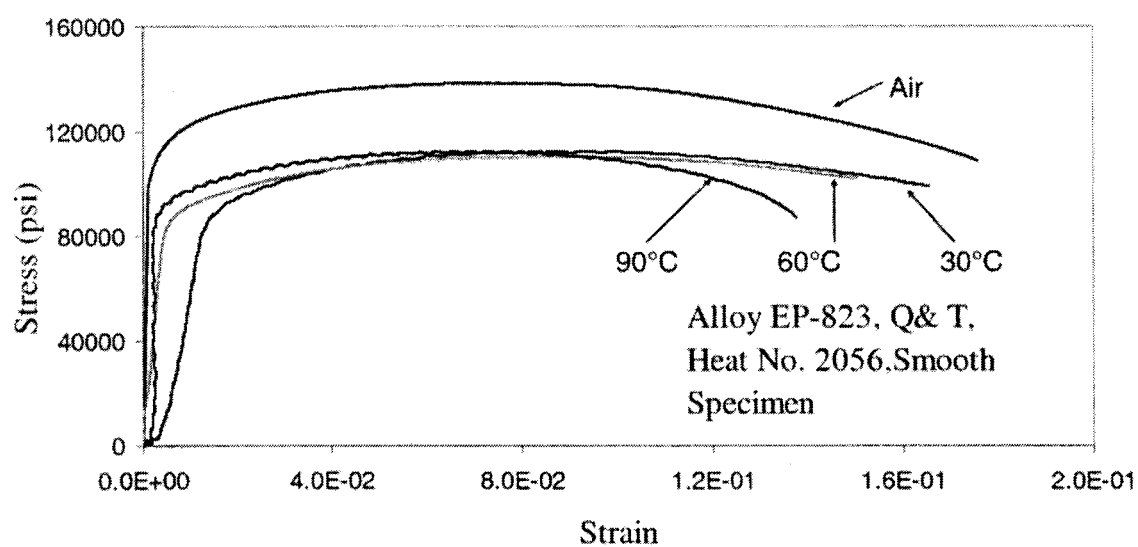


Figure 4.1 Comparison of Stress-Strain Diagrams in Neutral Solution

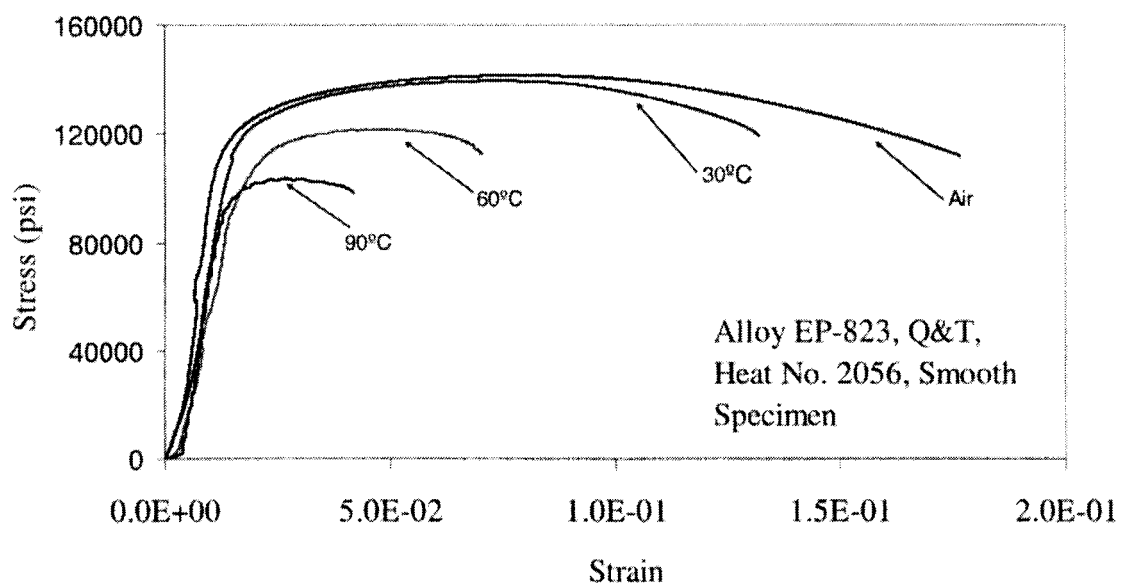


Figure 4.2 Comparison of Stress-Strain Diagrams in Acidic Solution

Table 4.3 SSR Test Results using Smooth Specimens

Alloy/ Heat No.	Environm ent.	Temperature (°C)	σ_f (ksi)	TTF (hours)	% El	% RA
EP-823/ 2056						
	Air	Ambient	187.3	24.2	26.4	72.5
	Neutral	30°C	182.5	22.6	24.3	64.3
		60°C	171.3	21.5	20.8	61.4
		90°C	120.6	15.5	15.3	28.8
	Acidic	30°C	159.0	21.0	20.7	57.4
		60°C	136.7	19.2	18.8	53.5
		90°C	101.6	11.9	11.6	26.4

σ_f : True Failure Stress

%El : Percentage Elongation

%RA : Percentage Reduction in Area

TTF : Time-To-Failure

The data presented in this table are an average value of two points that showed insignificant variation between the two.

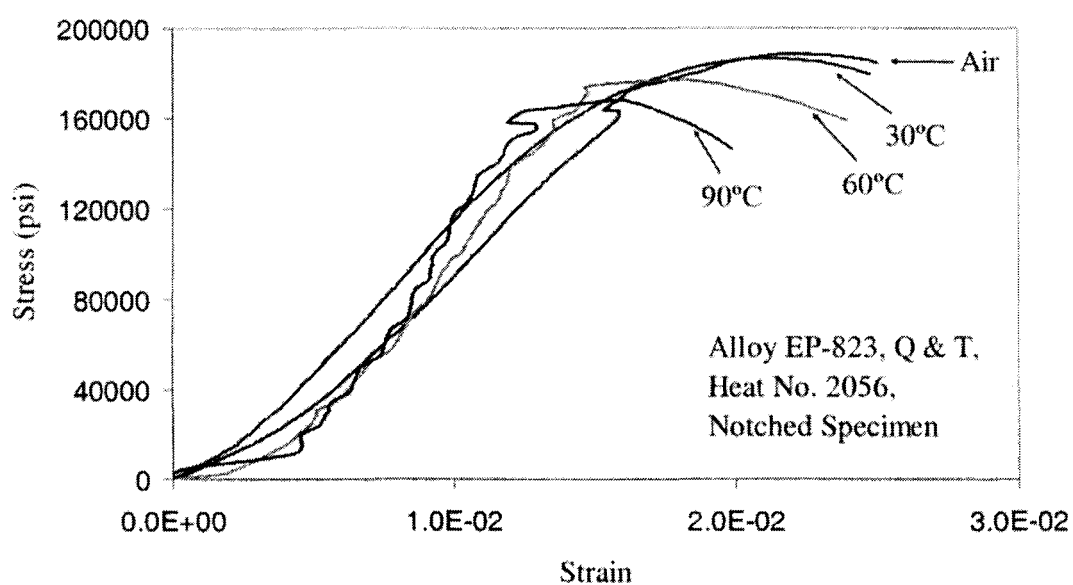


Figure 4.3 Comparison of Stress-Strain Diagram in Neutral Solution

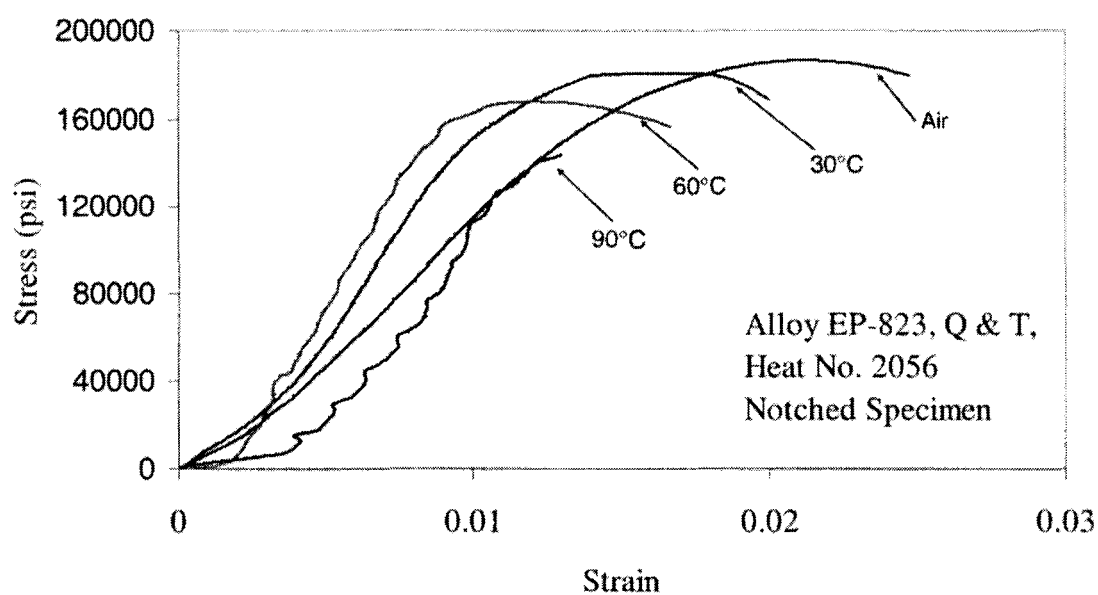


Figure 4.4 Comparison of Stress-Strain Diagram in Acidic Solution

Table 4.4 SSR Test Results using Notched Specimens

Environment	Temperature	σ_f (ksi)	TTF (hrs)	% El	% RA
Air	Room temp.	178.1	4.28	2.8	1.92
Neutral	30	183.1	4.14	2.5	1.60
	60	161.8	4.12	2.4	1.41
	90	148.4	4.11	2.3	1.28
Acidic	30	169.2	4.03	2.45	1.15
	60	156.9	4.00	2.41	1.08
	90	143.8	3.92	2.36	1.02

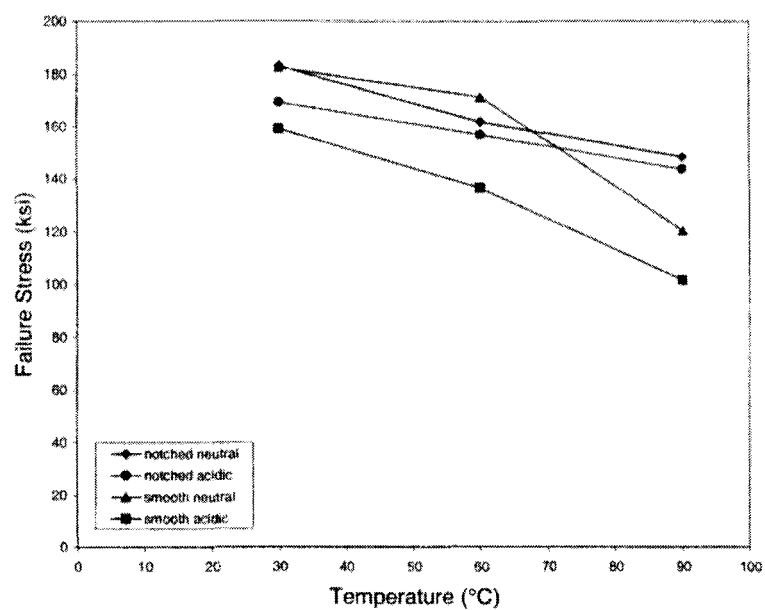


Figure 4.5 Effect of pH, Temperature and Specimen Geometry on σ_f

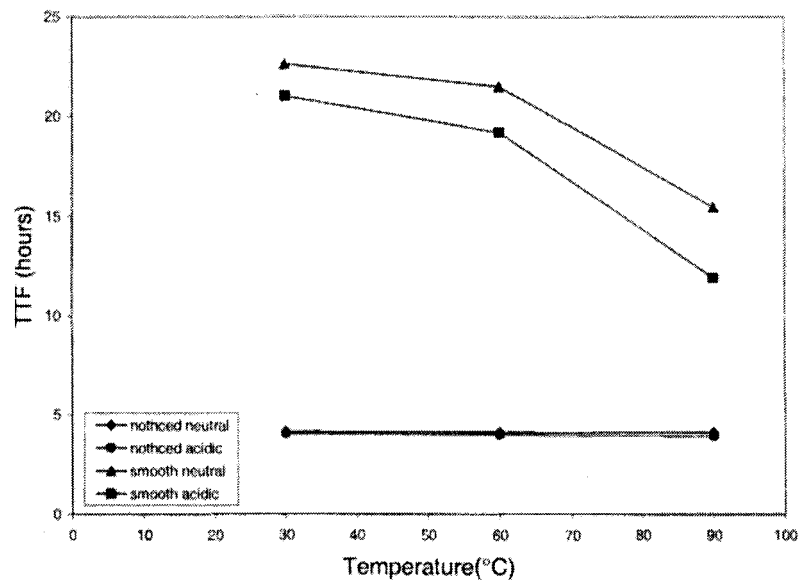


Figure 4.6 Effect of pH, Temperature and Specimen Geometry on TTF

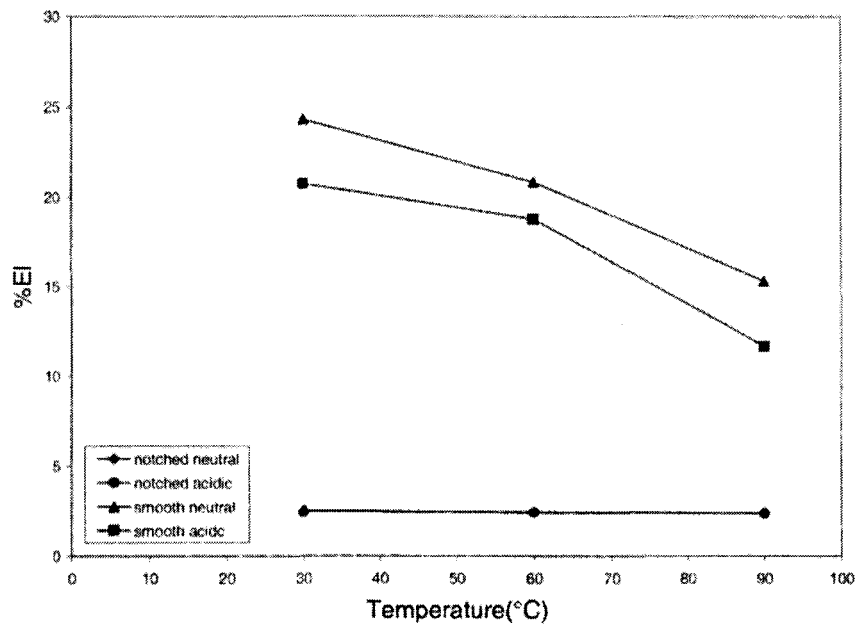


Figure 4.7 Effect of pH, Temperature and Specimen Geometry on %EI

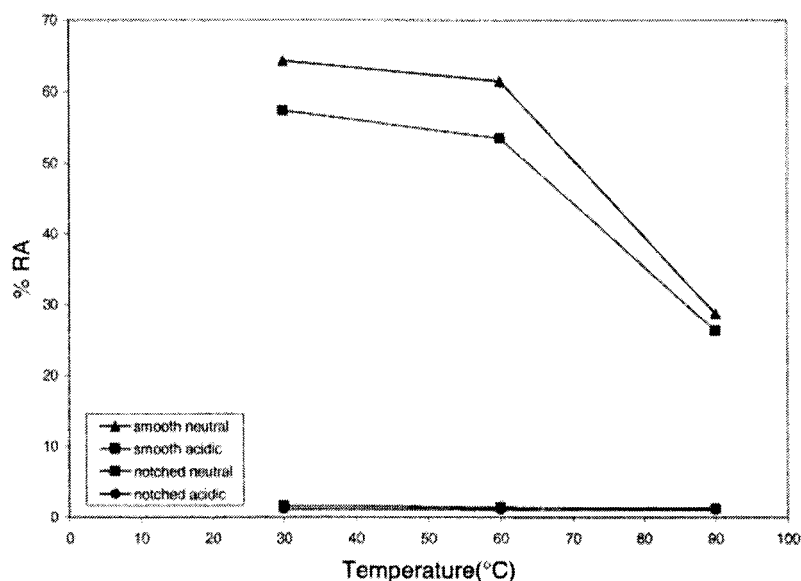


Figure 4.8 Effect of pH, Temperature and Specimen Geometry on %RA

4.3. SCC Testing using Self-Loaded Specimens

As indicated earlier in this thesis, an evaluation of the cracking susceptibility of Alloy EP-823 in the presence of molten LBE was of prime importance. However, the desired SCC testing using self-loaded specimens such as C-ring and U-bend could not be accommodated at LANL. SCC testing incorporating similar types of specimens were performed at UNLV in an acidic aqueous environment at ambient temperature, 50 and 100°C using either a desiccator (room temperature) or an autoclave (elevated temperatures).

One of the drawback of using C-ring and U-bend specimens to evaluate the SCC behavior of a material of interest is that the final load/stress experienced by either type of specimen cannot be controlled. In case of C-ring specimen, a desired deflection of the ring was given by changing its outer diameter through the application of a stress by

means of a bolt, based on the yield strength of the test material using Equation 2.2, shown in a previous section. However, in case of the U-bend specimen, the initial stress/load cannot be determined based on the specimen geometry. Thus, an arbitrary deflection between the two arms was given to produce stress in this type of specimen. Nevertheless, the evaluation of the SCC susceptibility using C-ring or U-bend specimens was based on the tensile stress experienced by the outer layer of either specimen type while being exposed to an aggressive environment such as an acidic solution used in this investigation. The C-ring specimens tested in this investigation were loaded by applying stresses on their outer layer corresponding to 95 and 98% of the YS value of Alloy EP-823.

The C-ring specimens were loaded by applying tensile stresses equivalent to 95 and 98% of the material's YS value. The results of SCC testing involving C-ring and U-bend specimens of Alloy EP-823 revealed no cracking at any testing temperature, irrespective of the applied stress level. Even though no cracks were observed in C-ring specimens at the end of 7 weeks of exposure, some crack-like indications were seen, as illustrated in Figure 4.9. No surface degradation was, however, observed with the U-bend specimens, showing shiny appearances upon completion of testing.



Figure 4.9 Comparison of C-Ring Specimen's appearance

4.4. SCC Testing at Controlled Potential

The susceptibility to hydrogen-induced cracking in Alloy EP-823 was determined by applying cathodic electrochemical potential (E_{cont}) to a cylindrical specimen while loaded in tension by the SSR technique. The magnitude of E_{cont} was based on the corrosion potential (E_{corr}) determined on a similar material by another investigator at UNLV.^[22] The results, shown in Figure 4.10, indicate that the magnitude of strain was reduced due to the application of E_{cont} , indicating reduced ductility. Simultaneously, the failure stress (σ_f) was also reduced due to cathodic charging, as illustrated in this figure.

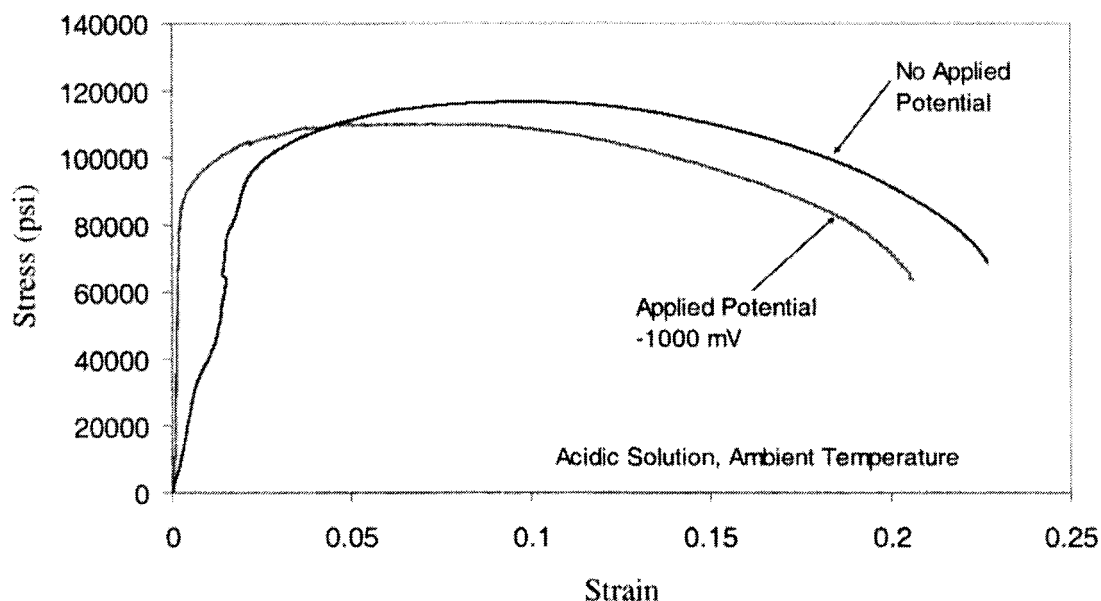


Figure 4.10 Acidic Environment, Ambient Temperature, $E_{\text{cont}} = -1000 \text{ mV}$

4.5. Results of Microscopic Evaluation

4.5.1. Optical Microscopy

Figure 4.11 illustrates the metallurgical microstructures of Alloy EP-823 following quenching and tempering. Examination of this figure confirms that fully-tempered and fine-grained martensitic microstructures were developed in this alloy. An examination of this micrograph also reveals the presence of delta ferrite (white particles) due to the presence of high chromium content in the test material. As shown earlier, ductility was significantly reduced in specimens loaded in tension while exposed to a 90°C acidic solution. An examination of the tested specimen in this environment revealed secondary cracks along the gage section of the broken specimen. Figure 4.12, illustrates the nature of secondary cracks, as determined by optical microscopy.

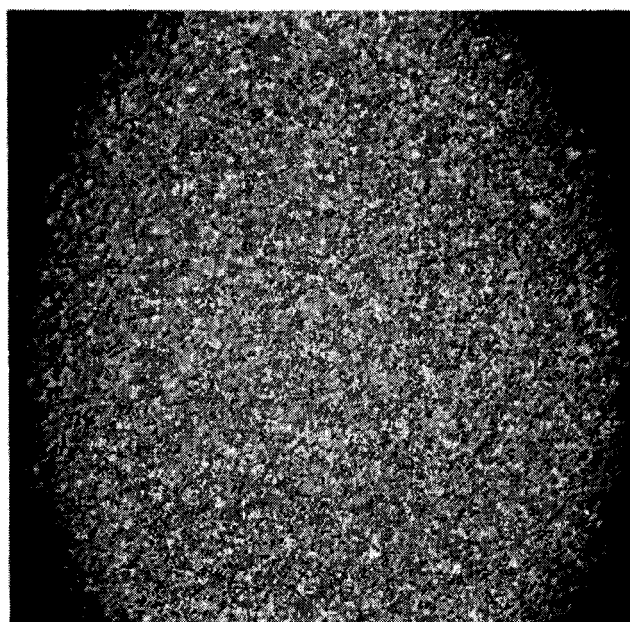


Figure 4.11 Microstructure of Q & T Alloy EP-823, Etched (Fry's Reagent), 10X

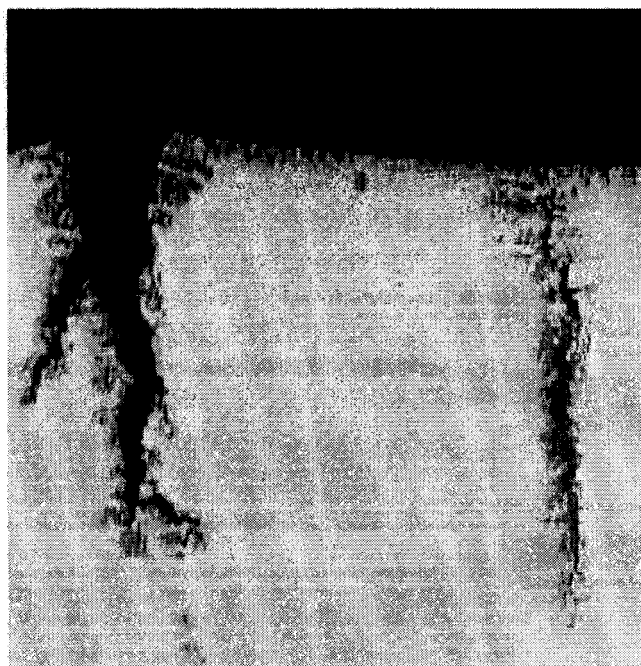


Figure 4.12 Secondary Cracks, 10X

4.5.2 Scanning Electron Microscopy

The results of SEM study are illustrated in Figures 4.13 through 4.15, showing the extent and morphology of failure in Alloy EP-823 tested in neutral and acidic solutions. An examination of the SEM micrograph shown in Figure 4.13 obtained in the neutral solution at ambient temperature indicate the presence of both ductile and brittle failures characterized by dimpled microstructure and intergranular cracking, respectively. However, at 90°C, transgranular brittle failures were also observed, as illustrated in Figure 4.14. The SEM micrograph obtained in the acidic solution at ambient temperature exhibits the presence of dimpled microstructure and intergranular cracking, as shown in Figure 4.15. A very similar fractographic characteristic was also observed in the 90°C acidic solution.

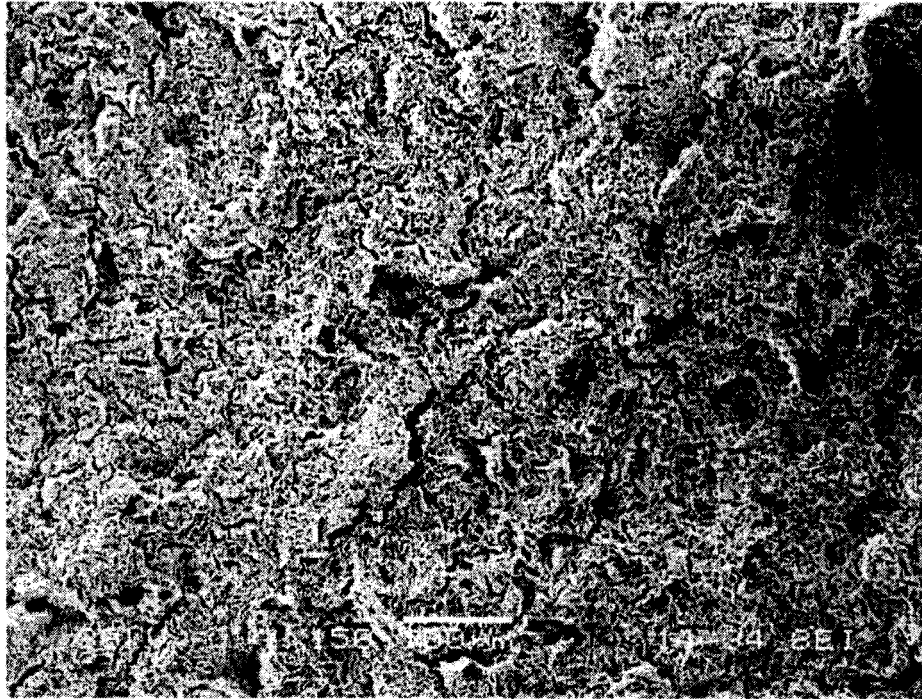


Figure 4.13 Ductile and Brittle Failures in Tensile Specimen at Ambient Temperature in Neutral Solution, 150X

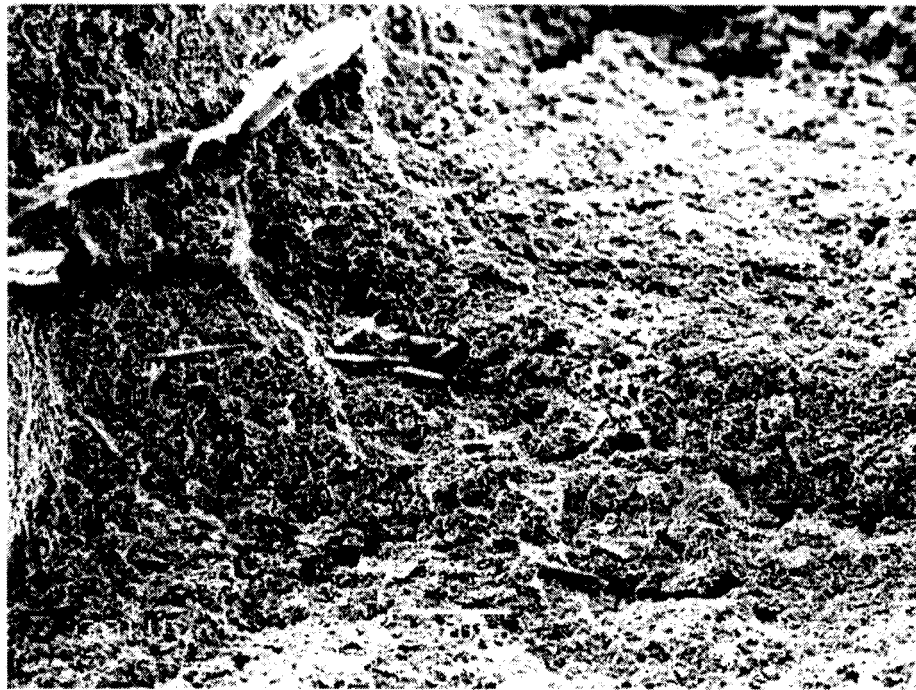


Figure 4.14 Ductile and Brittle Failures in Tensile Specimen in 90°C Neutral Solution, 150X

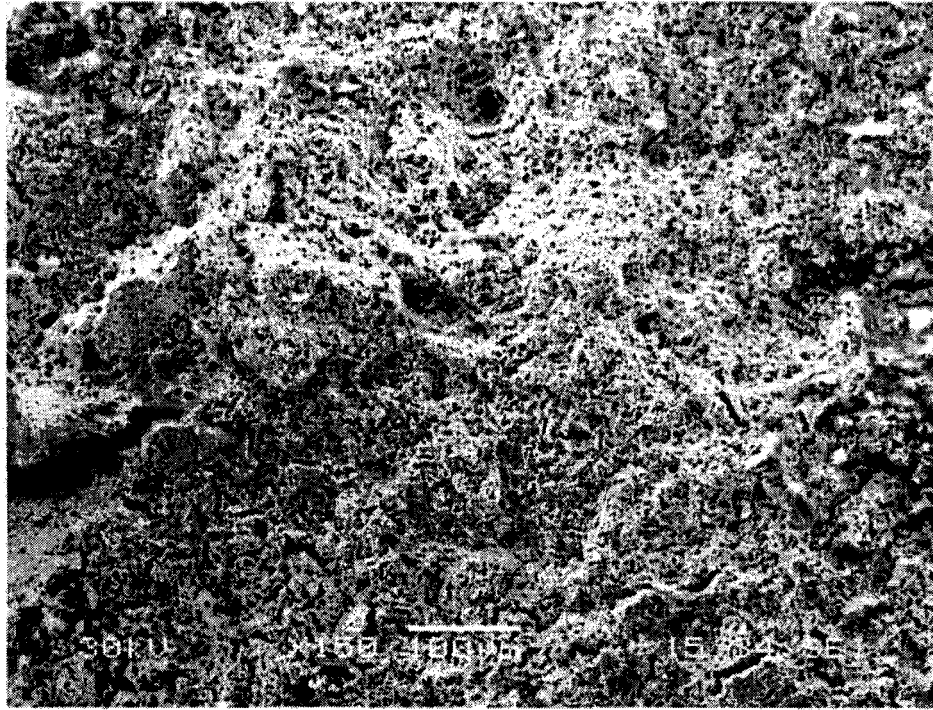


Figure 4.15 Ductile and Brittle Failures in Tensile Specimen at Ambient Temperature in Acidic Solution, 150X

CHAPTER 5

DISCUSSION

Martensitic Alloy EP-823 has been evaluated for its resistance to SCC and HE in neutral and aqueous environments at ambient and elevated temperatures. For SCC testing, both constant load and SSR techniques have been used. Since SCC testing involving self-loaded specimens could not be performed in the presence of molten LBE at LANL, SCC testing was performed at UNLV using C-ring and U-bend specimens in aqueous solutions. An effort was also made to study the effect of hydrogen on the cracking susceptibility of Alloy EP-823 by applying cathodic electrochemical potential to the test specimen under SSR condition. Micro-structural evaluations and characterizations of the secondary cracks in tensile specimens were performed by optical microscopy. Further, the extent and morphology of failure at the primary fracture face of the tested tensile specimen were determined by SEM. Brief discussions of the resultant data are presented in the next few sub-sections.

5.1. SCC – Constant-Load Testing

The results of SCC testing using smooth cylindrical specimens of Alloy EP-823 under constant loading conditions indicate that no failures may be experienced in either testing environment when loaded at a stress equivalent to 95% of the material's room temperature YS value. These results may indicate that the magnitude of σ_{th} for this alloy

may range between 95 and 100% the material's YS value. These data may also suggest that of all the three candidate alloys tested in the UNLV's research program, Alloy EP-823 may be the best target structural material for transmutation applications in terms of its resistance to SCC. The enhanced cracking resistance of Alloy EP-823 in the presence of an aggressive environment can be attributed to the formation of more protective oxide film, in particular, SiO_2 due to increased concentration of Si in this alloy compared to that in the other two alloys. (Alloy HT-9 and 422) incorporated in the Advanced Fuel Cycle Initiative (AFCI) program. It should, however, be mentioned that the presence of a notch in the cylindrical specimen reduced the σ_{th} value in the range of 45 to 50% of its YS value due to the detrimental stress-concentration effect. A similar effect of notch on the cracking susceptibility of engineering alloys has been reported by other researchers. [22, 26, 27]

5.2. SCC – SSR Testing

The results of SSR testing using both smooth and notched specimens indicate that, in general, the magnitude of strain was reduced with increasing temperature. This effect was more pronounced in the acidic solution. The data also indicate that parameters such as %El, %RA, TTF and σ_f were gradually reduced with increasing temperature, once again showing more pronounced effect in the acidic environment. This effect, which may be attributed to the synergistic effect of acidic pH and higher temperature, has been cited by other investigators. [22, 26, 27] Presence of notch further reduced these parameters, as expected. It is, however, interesting to note that the magnitude of σ_f was enhanced in the notched specimen due to the reduced cross-sectional area at the root of the notch and mechanical constraint resulting from the stress-concentration effect.

5.3. Self-Loaded SCC Testing

The results of SCC testing using C-ring and U-bend specimens of Alloy EP-823 in acidic solution at ambient and elevated temperatures indicate that this material may not undergo cracking even under these hostile environmental and highly-stressed conditions. The SCC data using C-ring specimens may indicate that given longer durations, some slight cracking might have been initiated in the outer stresses region of the C-ring specimens. Nevertheless, the U-bend specimens did not exhibit any degradations under any testing conditions.

5.4. SCC Testing under E_{cont}

The results of a limited number of SCC testing involving smooth specimens of Alloy EP-823 in the acidic solution at controlled cathodic potential indicate that the ductility parameters, TTF and σ_f were reduced to some extent. This phenomenon may be attributed to the generation of more hydrogen (H^+) ions in the acidic solution due to cathodic charging. The resultant data, showing a reduction in ductility, matches observations made by other investigators. [22-25, 28-32, 33-35]

5.5. Microscopic Evaluation

Metallographic evaluations by optical microscopy revealed conventional martensitic microstructures and branched secondary cracks along the gage section of the tested cylindrical specimens. An evaluation of the SEM micrographs reveals the presence of both ductile and brittle failures, characterized by dimples and intergranular/transgranular cracks, respectively. [36]

CHAPTER 6

SUMMARY AND CONCLUSIONS

Martensitic Alloy EP-823 has been proposed to be a candidate structural material to contain molten lead bismuth eutectic (LBE) during the transmutation process. This thesis presents the results of SCC testing of Alloy EP-823 in neutral and acidic solution at ambient and elevated temperatures. Constant load, SSR and self-loaded testing techniques have been used to evaluate the cracking susceptibility in this alloy. Further, the effect of hydrogen on cracking has also been investigated through application of cathodic electro-chemical potential to the test specimen while loaded in tension under SSR condition. Fractographic and metallographic evaluations of the tested specimens have been performed by SEM and optical microscopy respectively. The significant conclusions derived from this investigation are given below –

- Alloy EP-823 did not exhibit any failure at constant load in either test environment irrespective of temperature.
- The results of SCC testing using smooth specimen under SSR condition showed gradual reduction in TTF, σ_f and ductility parameters with increasing temperature showing more pronounced effect in the acidic solution. The presence of a notch, however, increased the magnitude of σ_f due to reduced cross-sectional area and plastic constraint at the root of the notch.

- Neither C-ring nor U-bend specimens of Alloy EP-823 showed cracks when tested in the acidic solution at ambient and elevated temperatures.
- The application of a -1000 mV potential to the test specimen in SSR testing reduced the magnitude of TTF, σ_f , %EI and %RA showing a detrimental effect of hydrogen generated due to cathodic charging on the cracking propensity.
- Secondary cracks were observed in the 90°C acidic solution along the gage section of the test specimen, as evidenced by optical micrograph.
- A combination of ductile and brittle failures was observed on the primary fracture face of the test specimen, as determined by SEM.
- An analysis of the overall data involving alloys EP-823, HT-9 and 422 in the AFCI research program clearly indicates that Alloy EP-823 would be the most viable target structural material in view of its superior metallurgical and corrosion properties due to the presence of higher silicon content.

CHAPTER 7

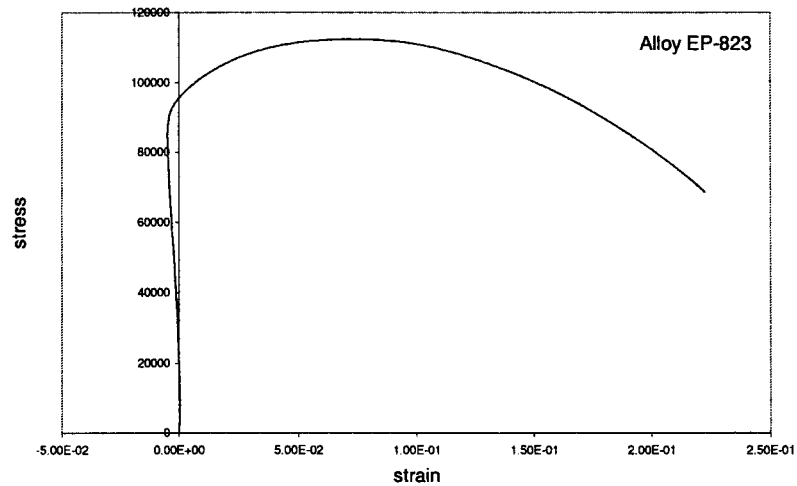
FUTURE WORK

Since testing could not be performed involving Alloy EP-823 in the presence of molten LBE, it is suggested that comprehensive metallurgical and corrosion studies be performed either at UNLV or LANL in future using molten LBE as the testing environment.

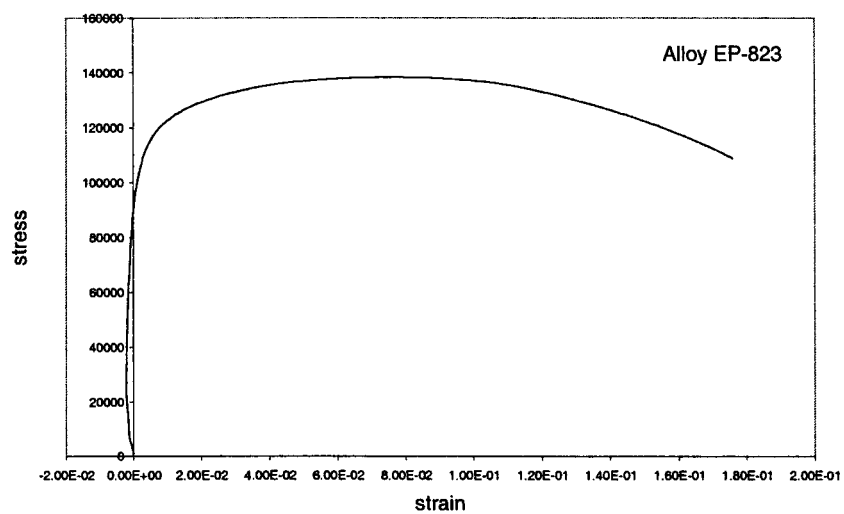
APPENDIX

SLOW-STRAIN-RATE DATA

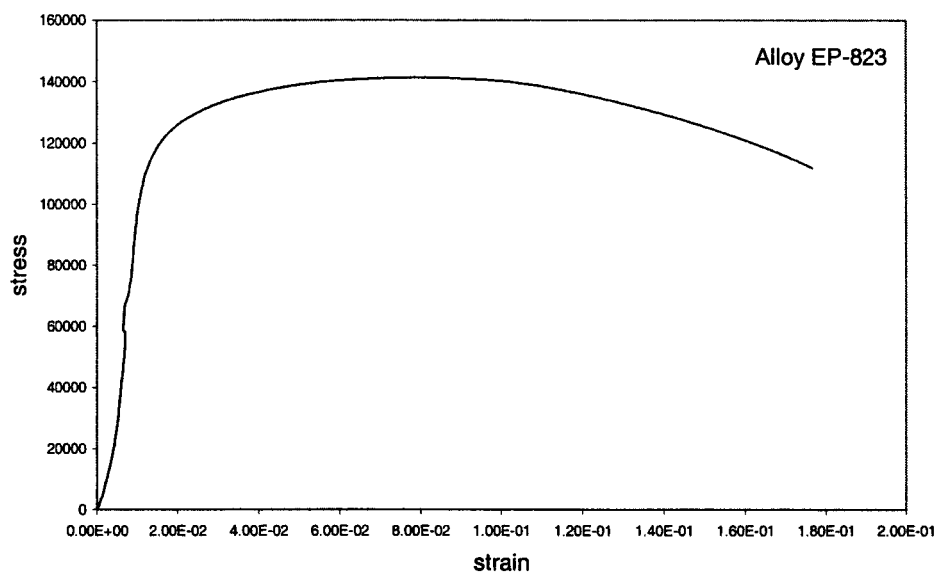
1. Stress versus Strain Curves (Smooth Specimens)



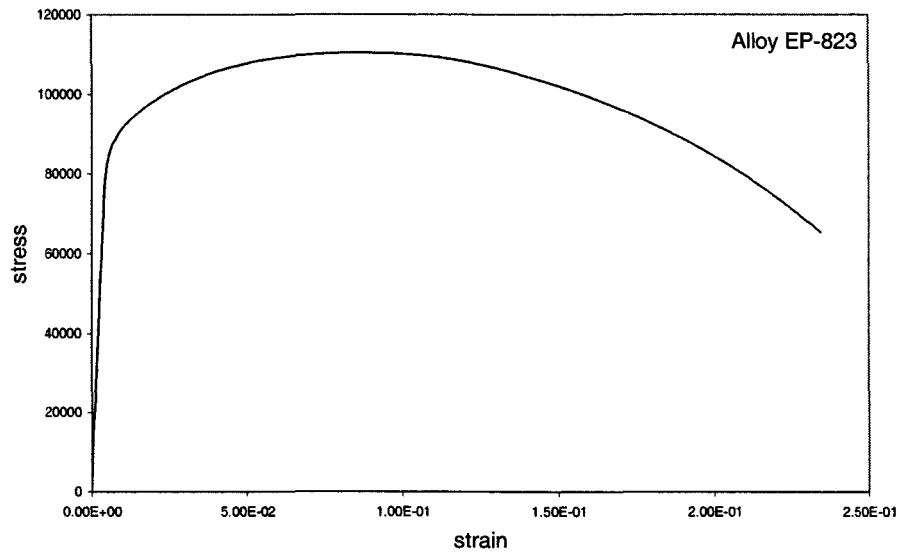
Air (Smooth Sample 1)



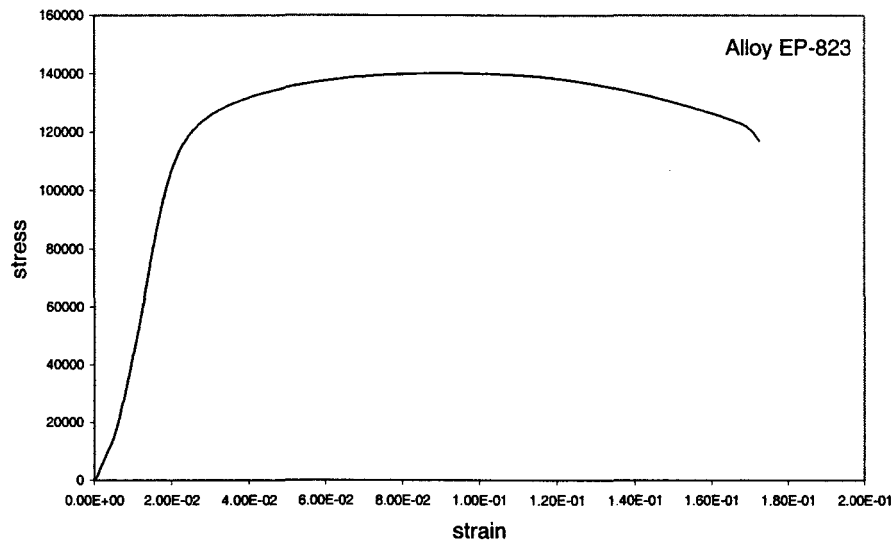
Air (Smooth Sample 2)



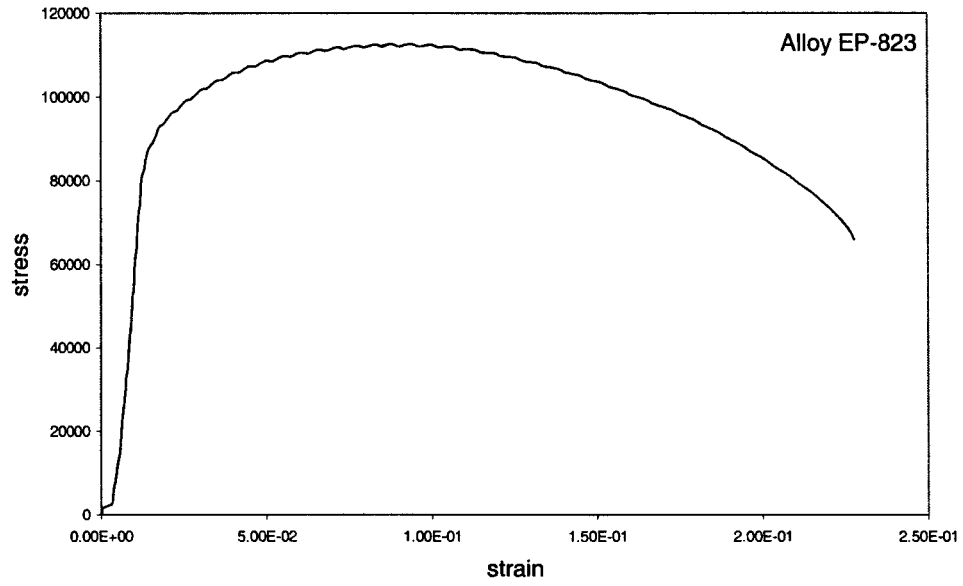
Air (Smooth Sample 3)



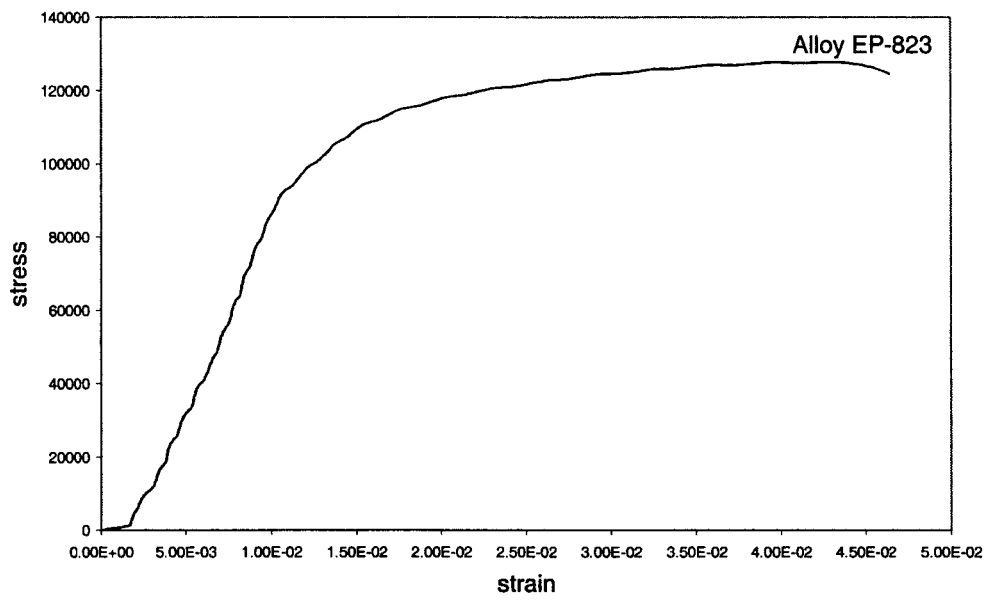
Neutral Environment, Ambient Temperature (Smooth Sample 1)



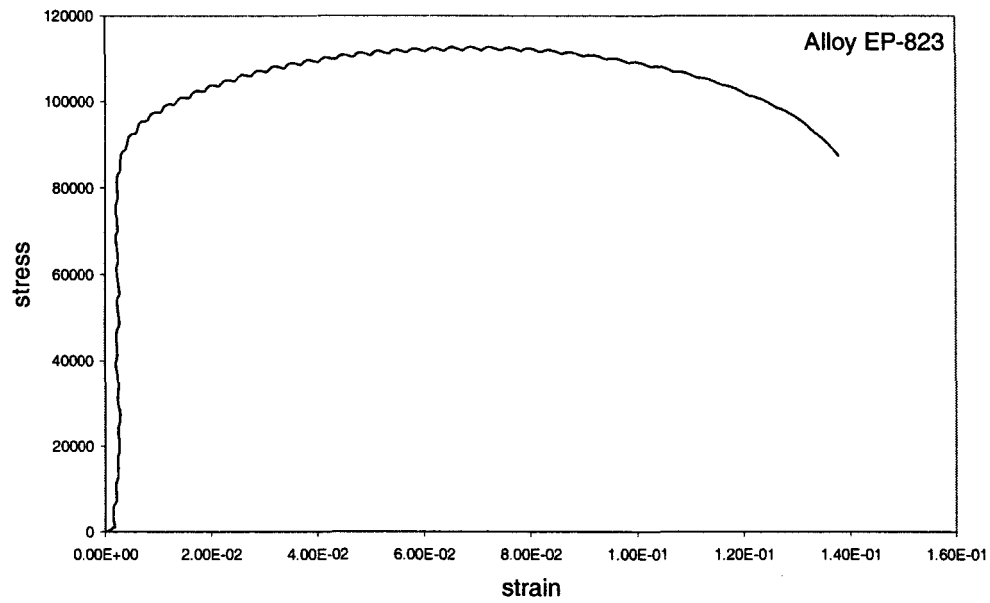
Neutral Environment, Ambient Temperature (Smooth Sample 2)



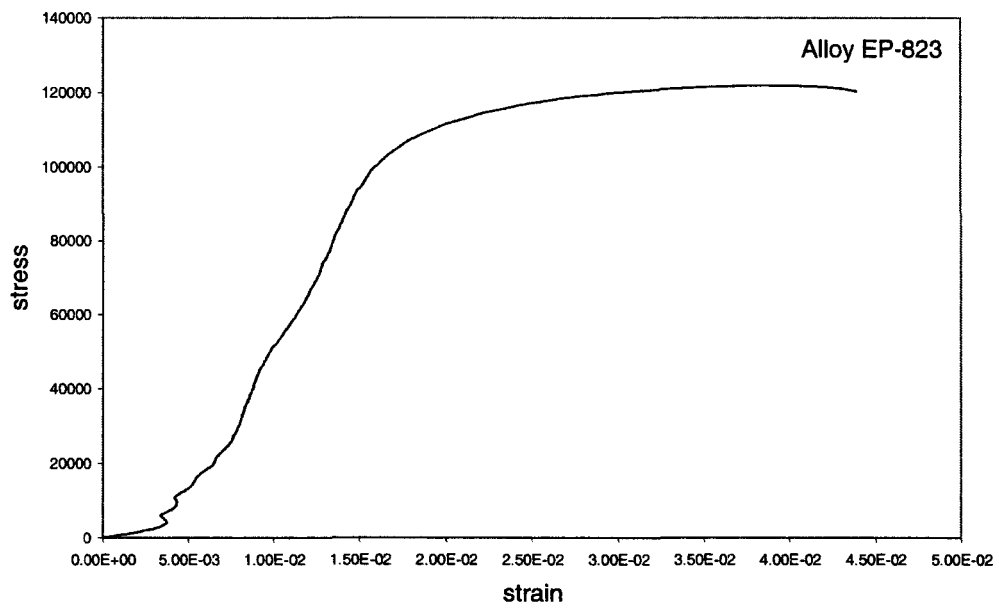
Neutral Environment, 60°C (Smooth Sample 1)



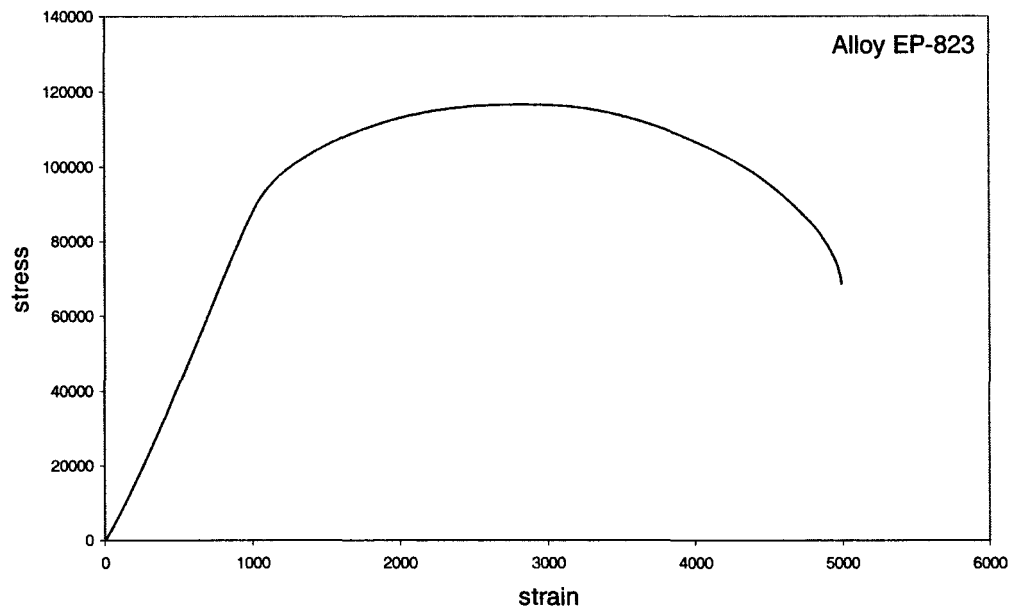
Neutral Environment, 60°C (Smooth Sample 2)



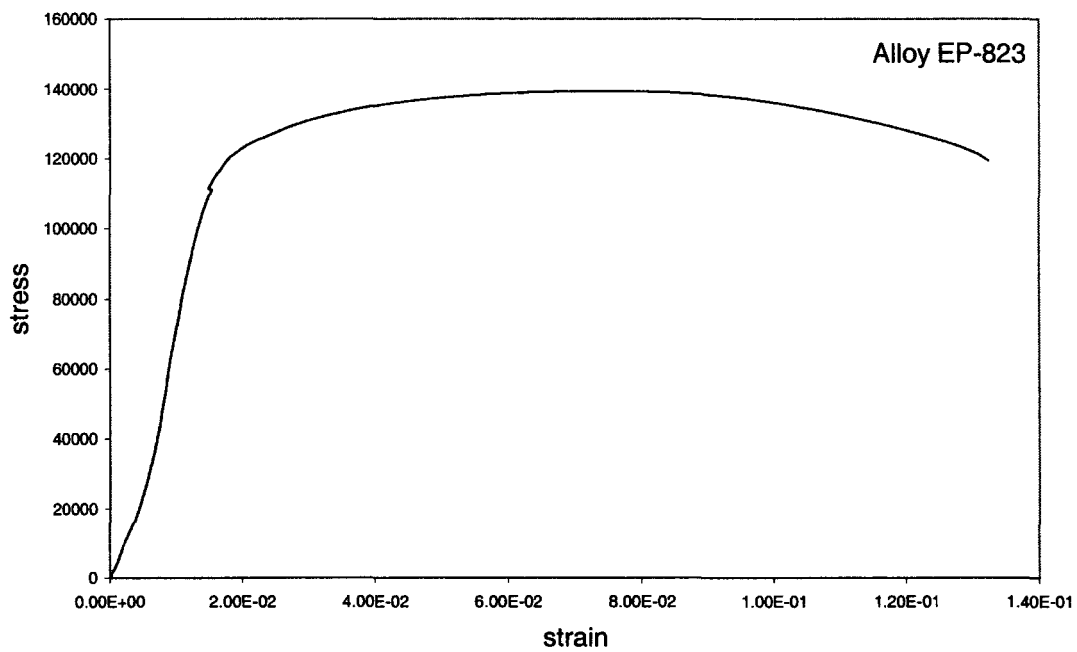
Neutral Environment, 90°C (Smooth Sample 1)



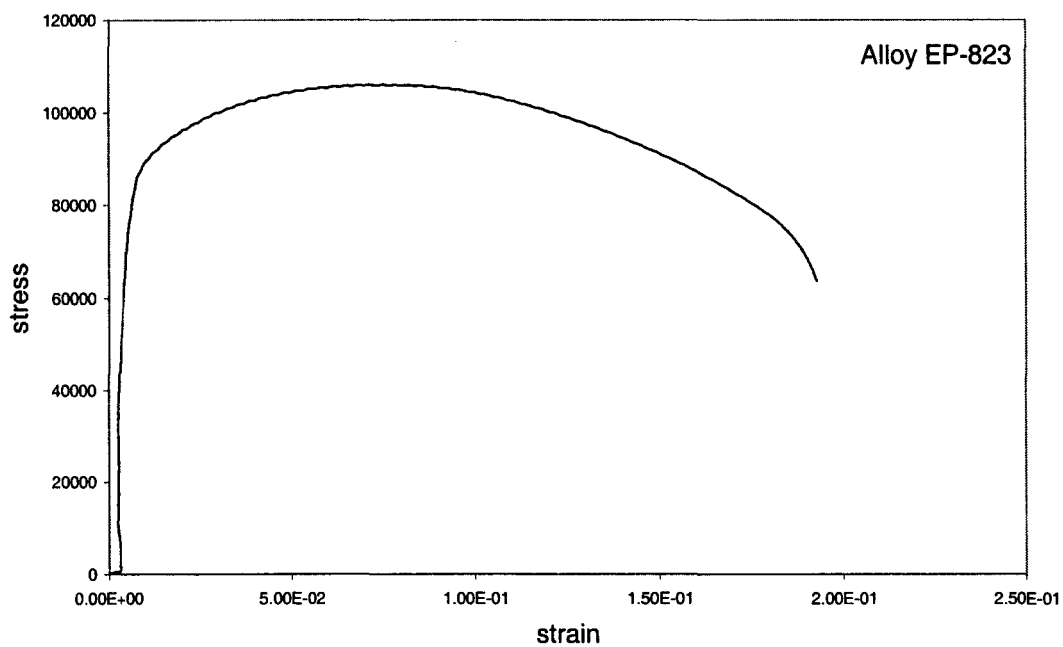
Neutral Environment, 90°C (Smooth Sample 2)



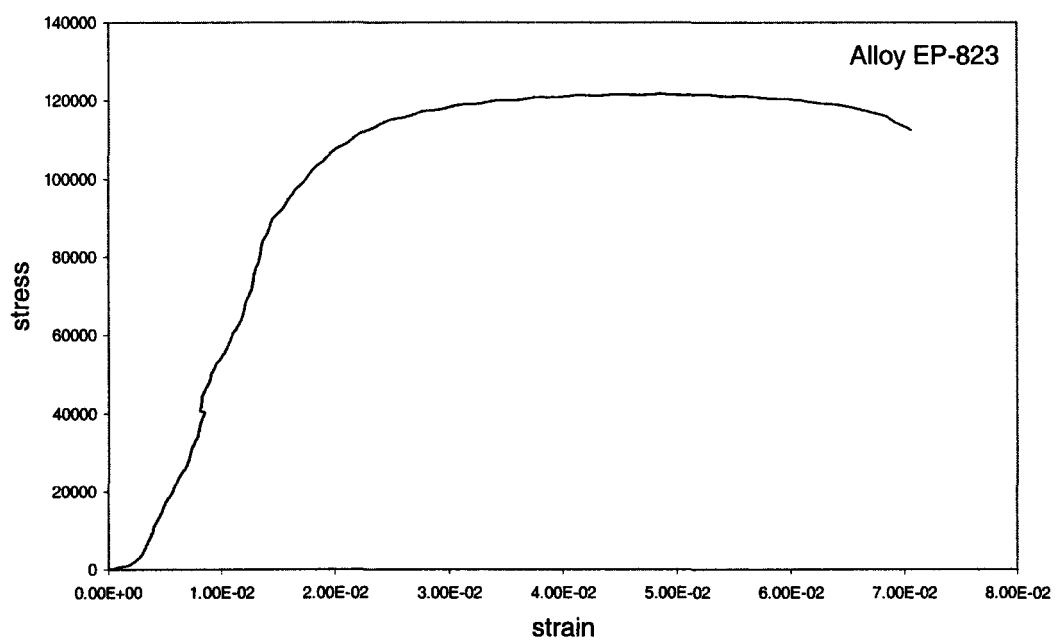
Acidic Environment, Ambient Temperature (Smooth Sample 1)



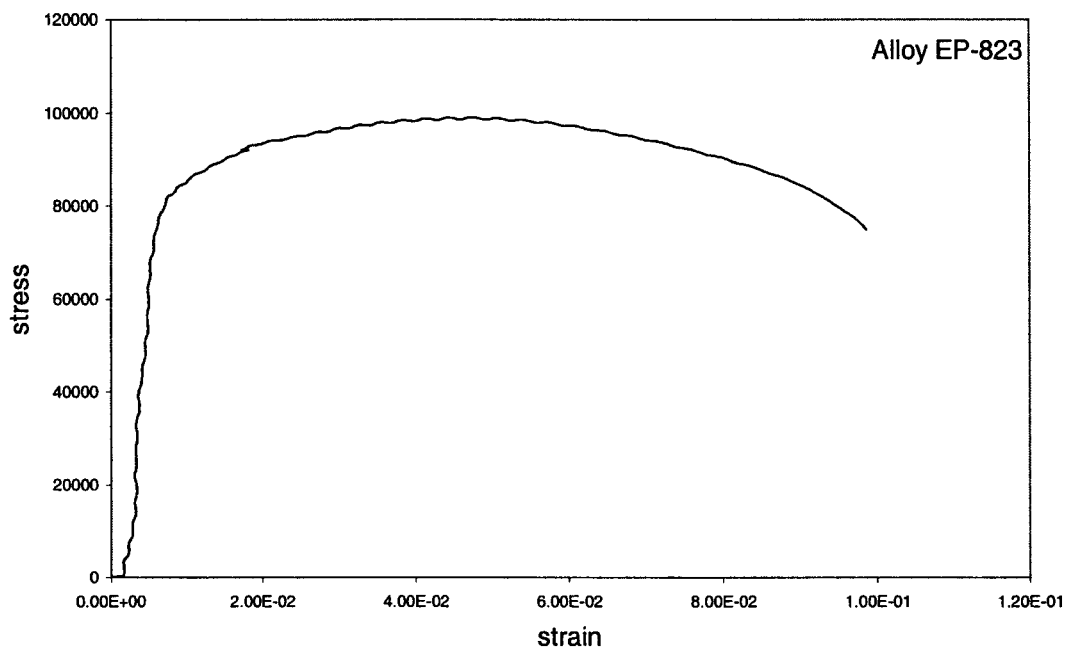
Acidic Environment, Ambient Temperature (Smooth Sample 2)



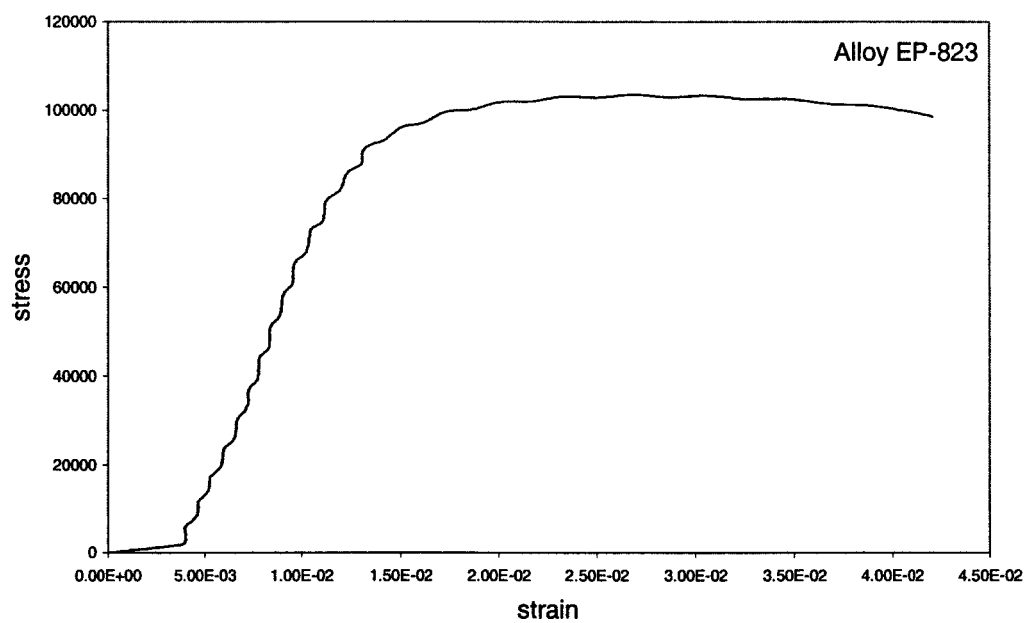
Acidic Environment, 60°C (Smooth Sample 1)



Acidic Environment, 60°C (Smooth Sample 2)

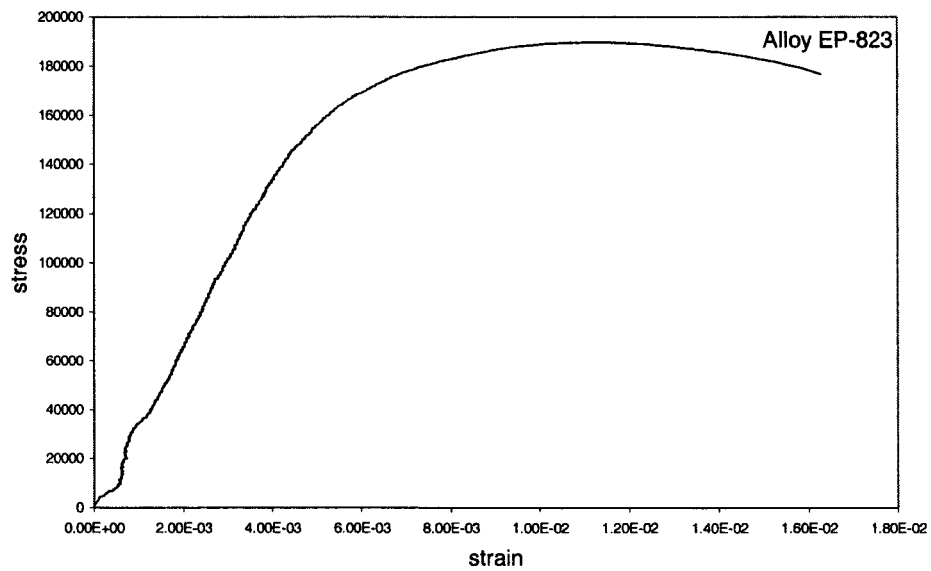


Acidic Environment, 90°C (Smooth Sample 1)

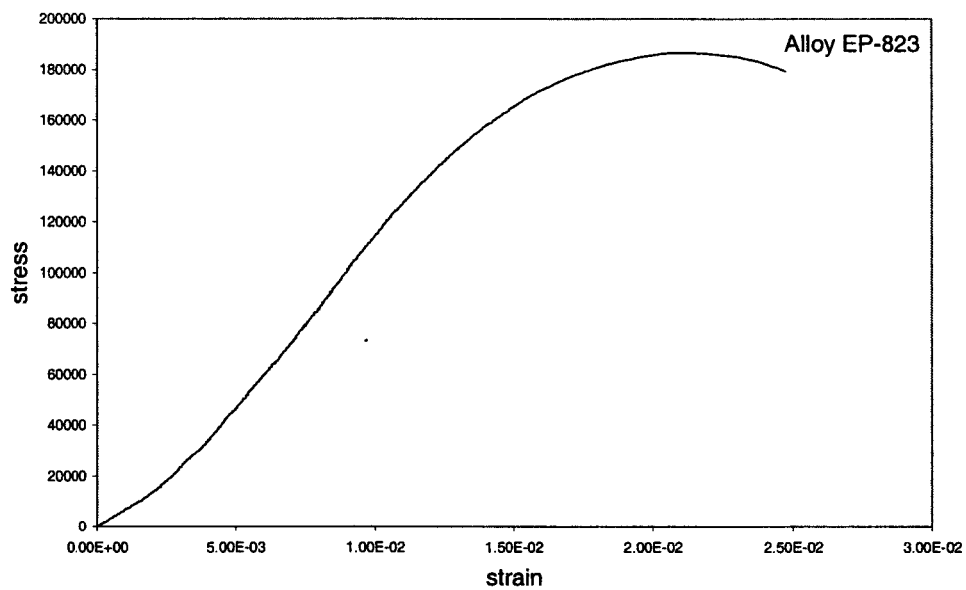


Acidic Environment, 90°C (Smooth Sample 2)

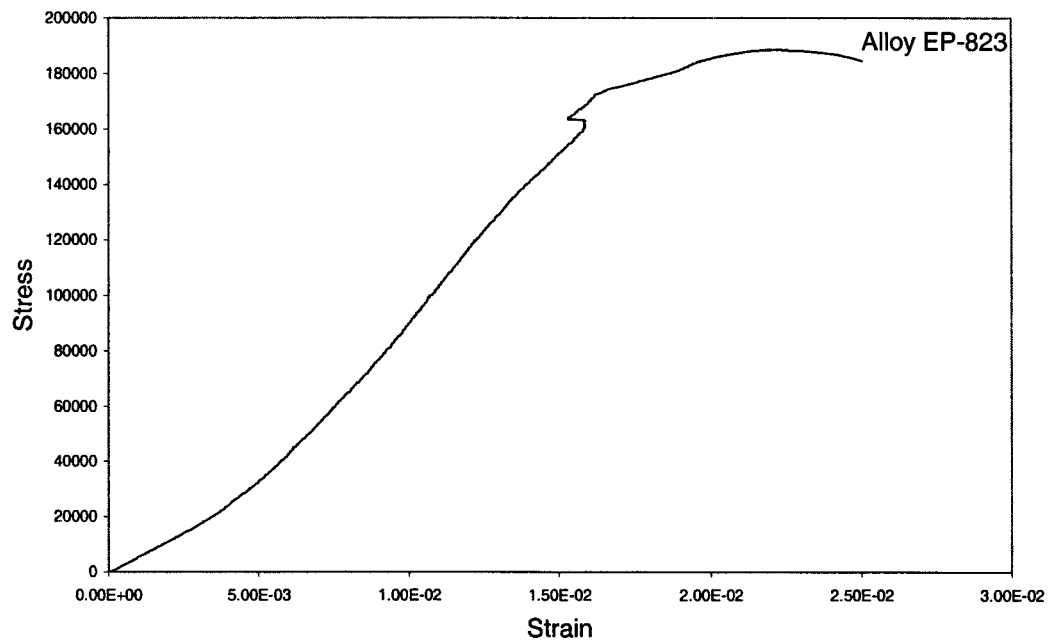
2. Stress versus Strain Curves (Notched Specimens)



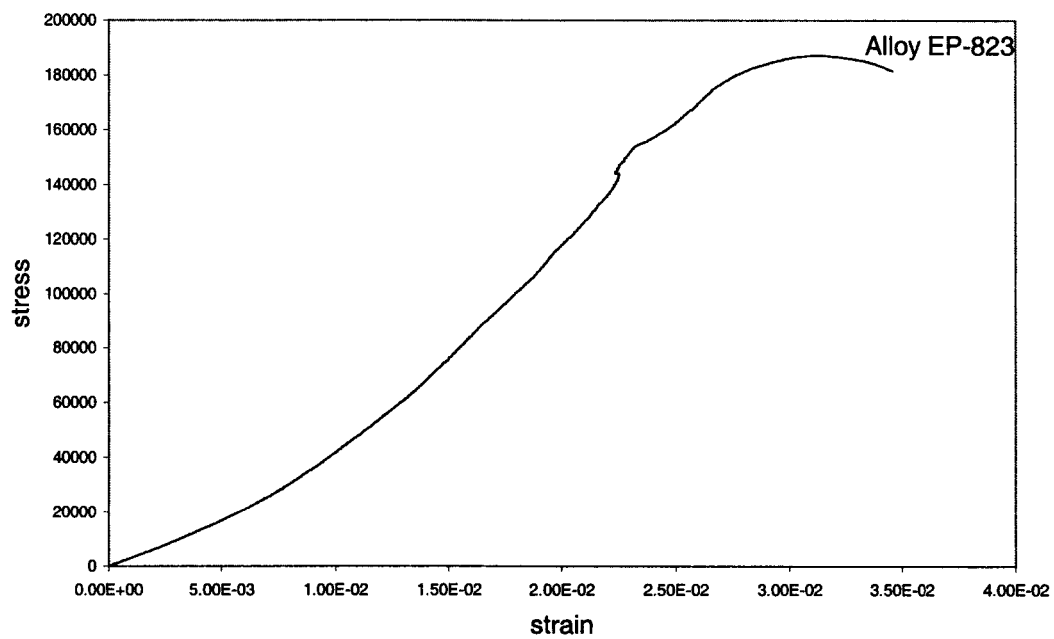
Air (Notched Sample 1)



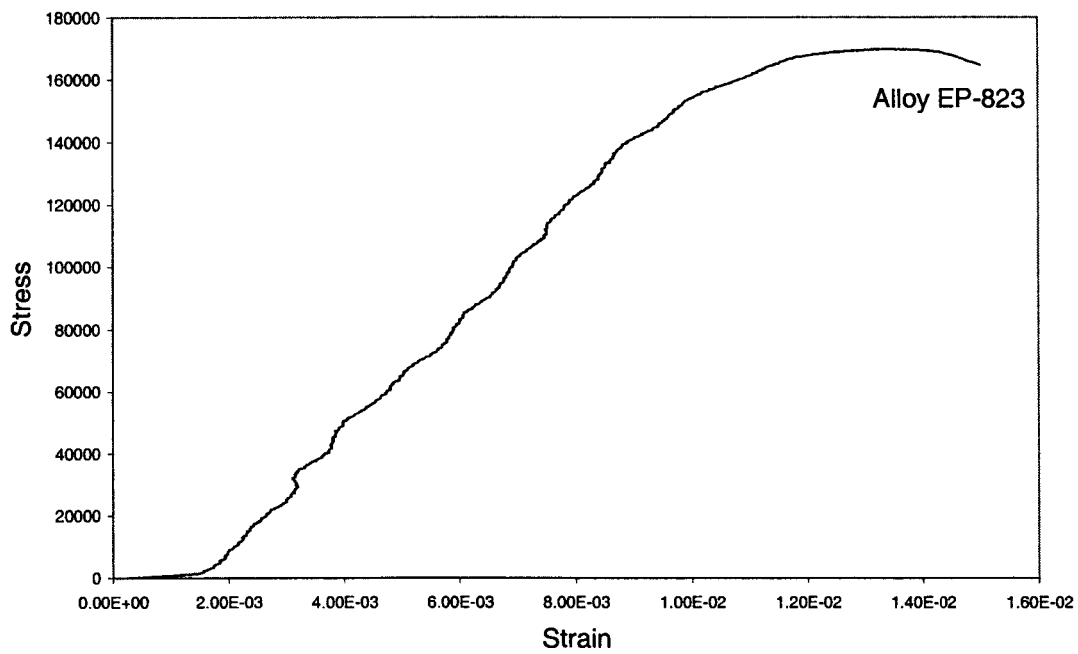
Air (Notched Sample 2)



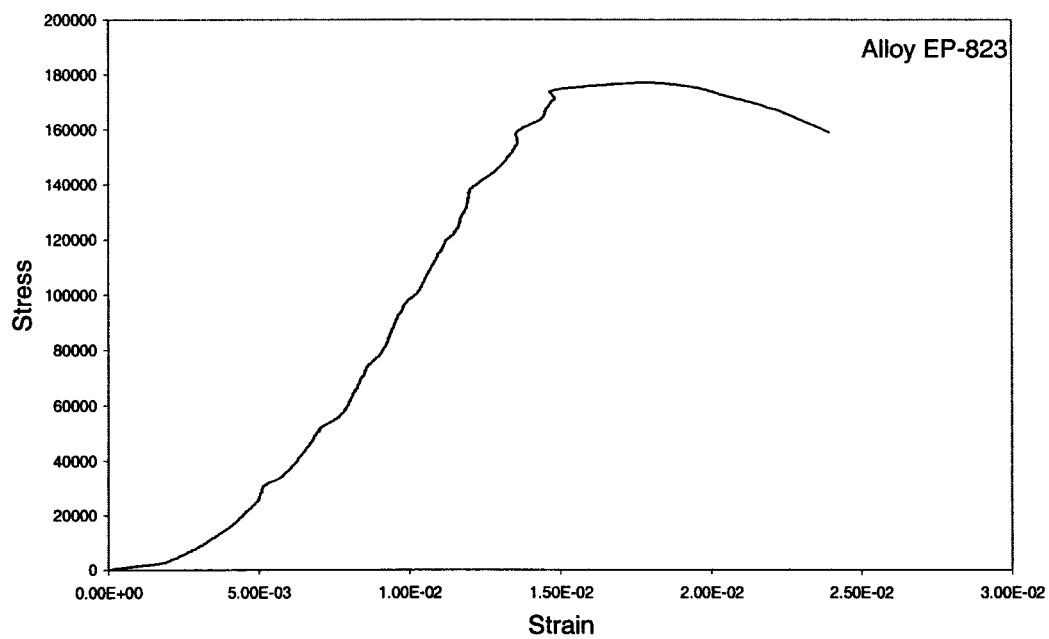
Neutral Environment, Ambient Temperature (Notched Sample 1)



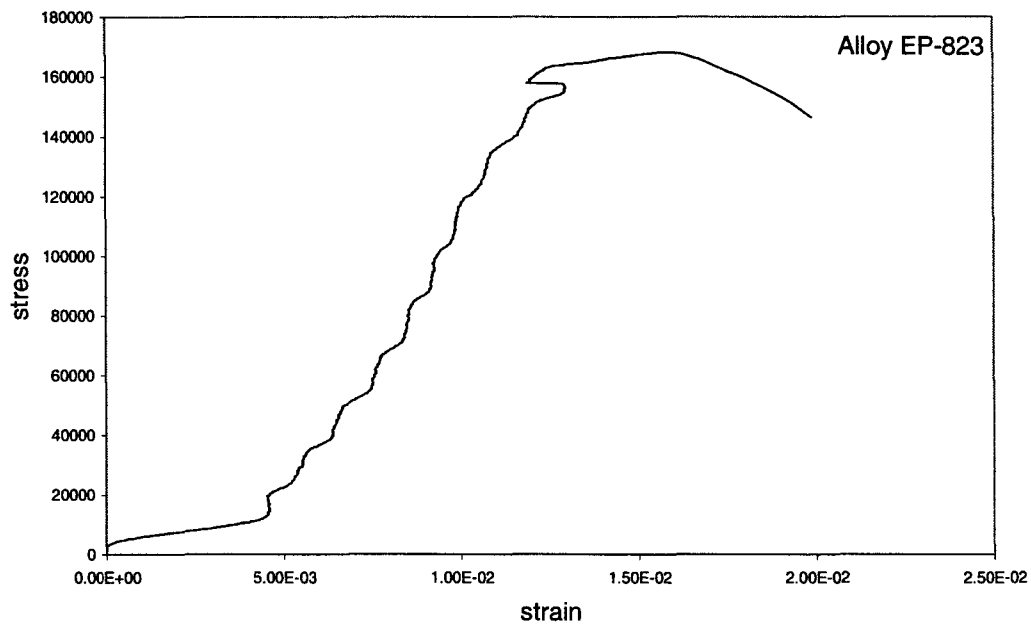
Neutral Environment, Ambient Temperature (Notched Sample 2)



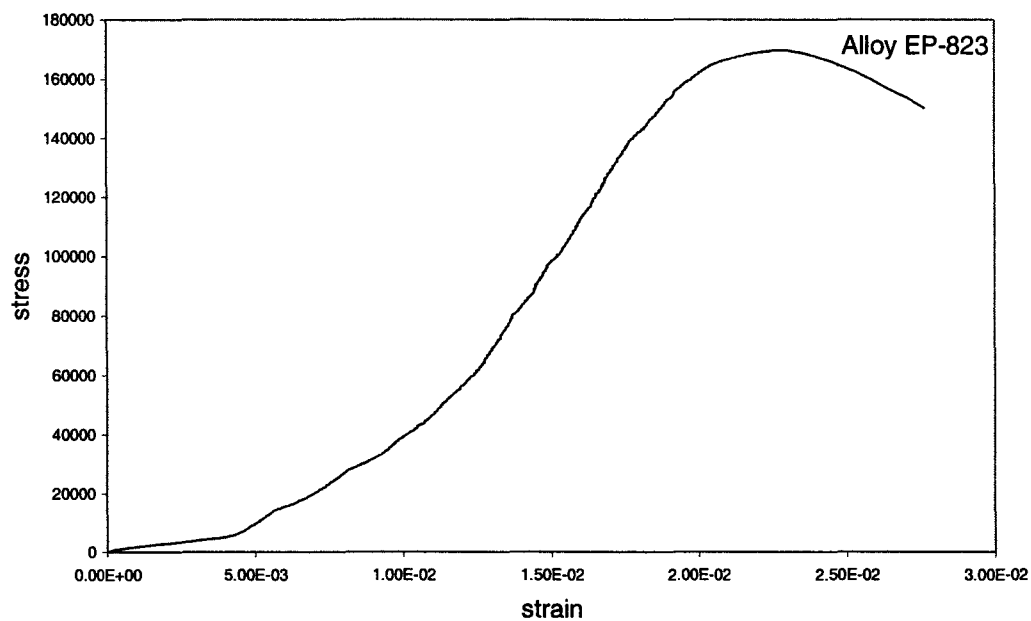
Neutral Environment, 60°C (Notched Sample 1)



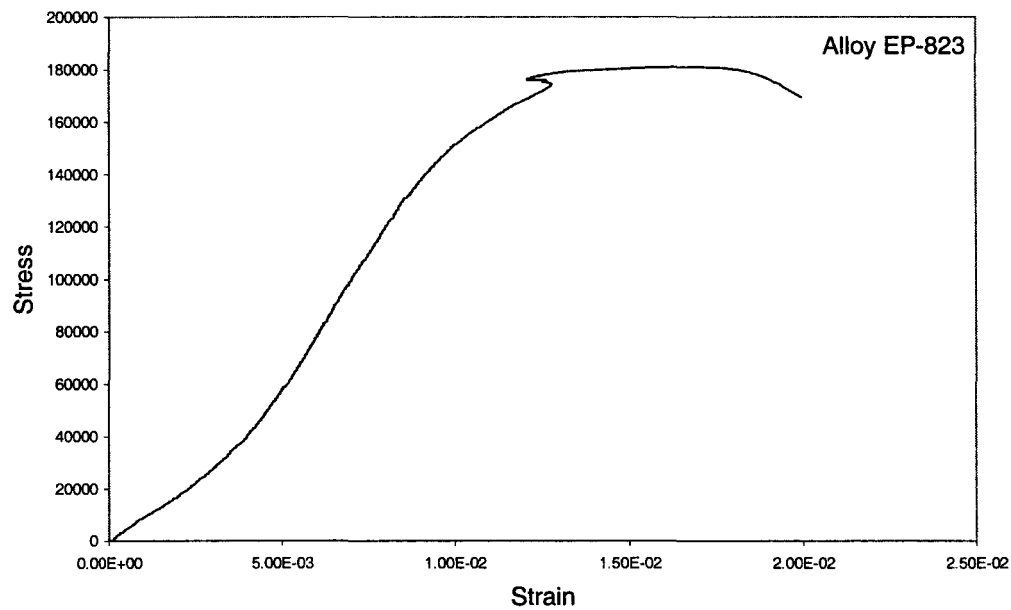
Neutral Environment, 60°C (Notched Sample 2)



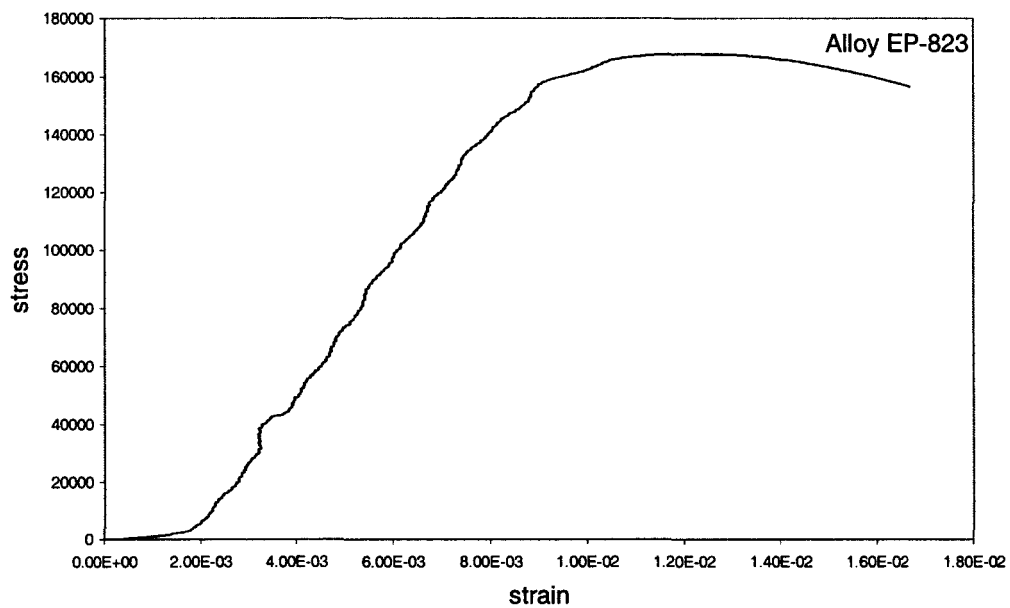
Neutral Environment, 90°C (Notched Sample 1)



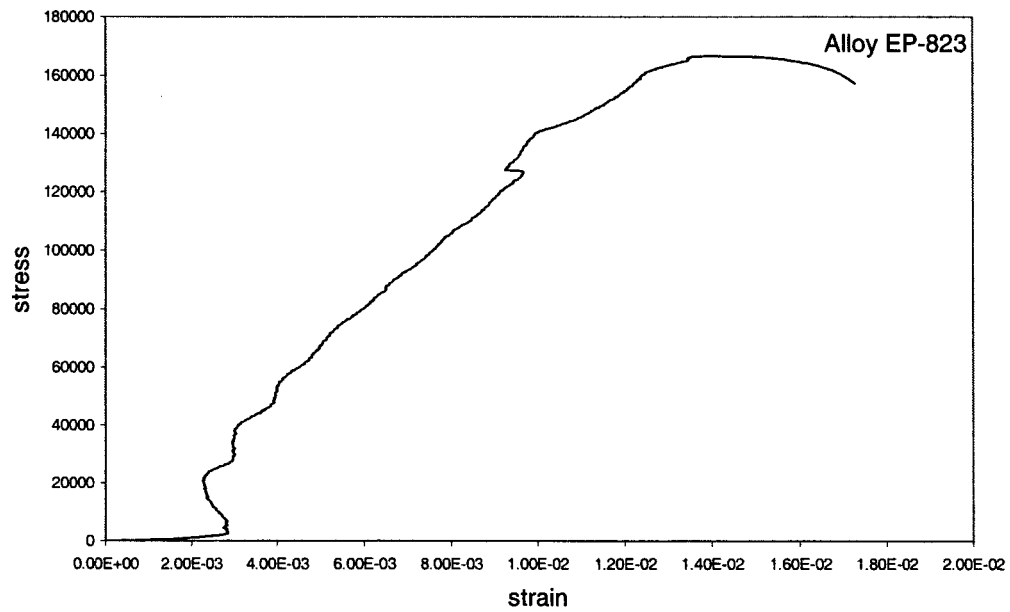
Neutral Environment, 90°C (Notched Sample 2)



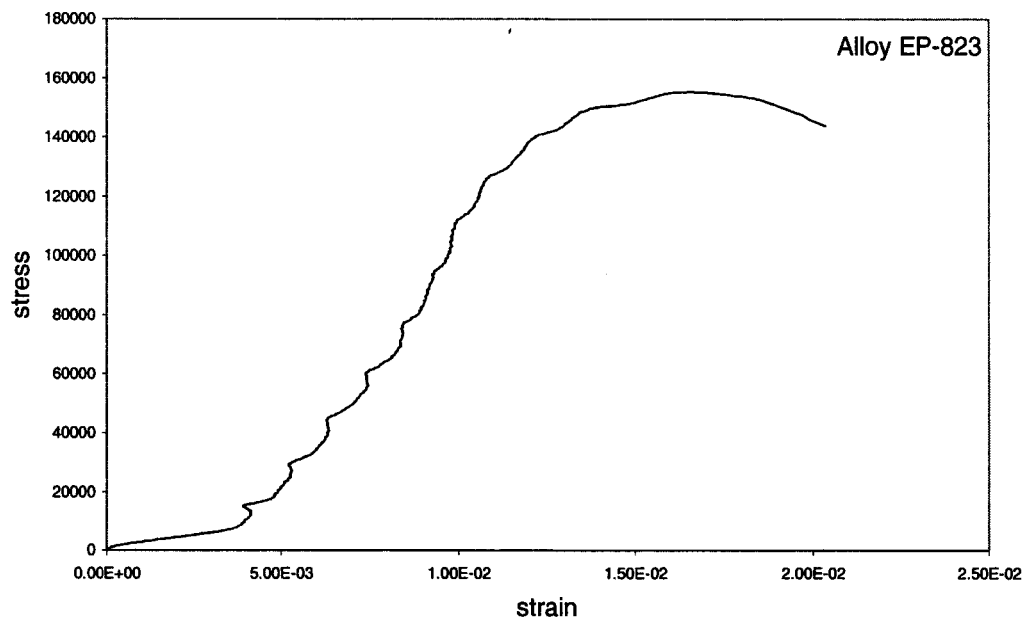
Acidic Environment, Ambient Temperature (Notched Sample 1)



Acidic Environment, 60°C (Notched Sample 1)



Acidic Environment, 60°C (Notched Sample 2)



Acidic Environment, 90°C (Notched Sample 1)

BIBLIOGRAPHY

1. S. Chwaszczewski, et al., "Transmutation of radioactive waste", *Applied Energy*, 75, pp. 87-96 (2003)
2. Mustafa Ubeyli, "Transmutation of minor actinides discharged from LMFBR spent fuel in a high power density fusion reactor", *Energy Conversion and Management*, article in press (2004)
3. Office of Civilian Radioactive Waste Management Program Briefing, Yucca Mountain Project, US Department of Energy
4. S. Leray, "Nuclear Waste Transmutation", Nuclear Instruments and Methods in Physics Research, Section B: Beam Interactions with Materials and Atoms, v 13, n 1-4, pp. 495-500 (Jun 1, 1996)
5. Ning Li et al., "Lead Bismuth Eutectic Materials Test Loop" , Los Alamos National Laboratory (August 2001)
(www.lanl.gov/lead-bismuth_eutectic)
6. George E. Dieter., Mechanical Metallurgy, pp. 496-500, (1998)
7. D.H. Mesa, A. Toro, et al., "The Effect of Testing Temperature on Corrosion-Erosion Resistance of Martensitic Steels".
8. Mechanical Properties of Stainless Steel, Outokumpu Stainless Website
(http://www.outokumpu.com/pages/page_5832.aspx)
9. H.E. Boyer (Ed.), Metals Handbook, vol 10, American Society for Metals, Metals Park, Ohio, pp. 217-218 (1975)
10. Kimura, A. and H. Matsui, "Neutron Irradiation Effects on the Microstructure of Low-Activation Ferritic Alloys", *Journal of Nuclear Materials*, 701, pp. 212-215, (1994)
11. V.S. Khabarov, V.D. Dmitriev et al., "Mechanical Properties and Microstructure of Neutron-Irradiated Ferritic-Martensitic Steel, used as Wrapper Material for the BN-350 and BN-600 Fast Reactor", *Proceedings of International Conference*,

- “Fast Reactor Core and Fuel Structural Behavior”. Inverness, pp. 263-267 (4-6 June 1990)
12. A.G. Ioltukhovski, et al., “Material Science and Manufacturing of Heat-Resistant Reduced Activation Ferritic-Martensitic Steels for Fusion”, *Journal of Nuclear Materials*, pp. 283-287 (2000)
 13. S.I. Porollo, Yu. V. Konobeev and A.M. Dvoriashin (State Scientific Center of Russian Federation, The Institute of Physics and Power Engineering, 249020 Obninsk, Russia) N.I. Budylnin, E.G. Mironova, M.V. Leontyeva-Smirnova, A.G. Ioltukhovskiy (State Scientific Center of Russian Federation, A.A. Boinchvar All-Russia Research Institute of Inorganic Materials (VNIINM), Moscow, Russia) and F.A. Garner (Pacific Northwest National Laboratory) “Irradiation Creep and Mechanical Properties of Two Ferritic-Martensitic Steels Irradiated in the BN-350 Fast Reactor”
 14. Zihni Ozturk, Monroe S. Wechsler, “Effects of High Energy Protons on the Mechanical Properties of Fe-2.25Cr-1Mo and Fe-12Cr-1Mo Steels”, *Transactions of the Journal of Engineering and Environmental Science*, 22 , pp. 197-202 (1998)
 15. R.C. Juvinall, et al., “Stress Concentration Factors for Grooved Shafts with Axial Loading”, *Fundamentals of Machine Component Design*, pp. 144 (1999)
 16. ASTM G38-01, “Standard Practice for Making and Using C-Ring Stress-Corrosion Test Specimens”
 17. ASTM G30-97, “Standard Practice for Making and Using U-Bend Stress-Corrosion Test Specimens”
 18. Ajit K. Roy, Mohammad K. Hossain, Brendan J. O’Toole, “Stress Corrosion Cracking of Martensitic Stainless Steels for Transmutation Applications”, *The 10th International High-Level Radioactive Waste Management Conference*, Paper No. 69425, Las Vegas, NV, March 30-April 3 (2003)
 19. P. Jung, C. Liu, J. Chen, “Retention of Implanted Hydrogen and Helium in Martensitic Stainless Steels and their Effects on Mechanical Properties”. *Journal of Nuclear Materials*, 296, pp. 165-173 (2001)
 20. Cortest, Incorporated Website (www.cortest.com)
 21. Ajit K. Roy et al., “Cracking of Titanium Alloys under Cathodic Applied Potential”, *Micron*, vol 32, No. 2, Elsevier Science, pp. 211-218 (February 2001)
 22. Mohammad K. Hossain, Thesis, “Stress Corrosion Cracking and Hydrogen Embrittlement of Martensitic Alloy EP-823” , (Dec 2004)

23. Hydrogen Embrittlement, Corrosion Source Website
(http://www.corrosionsource.com/handbook/CPS/cps_a_hic.htm)
24. I. Azkarate, et al., "Hydrogen Assisted Stress Cracking of Titanium Alloys in Aqueous Chloride Environments", *Progress in the Understanding and Prevention of Corrosion*, 2, Spain, pp. 1573-1580 (1993)
25. A. K. Roy, et al., "Effect of Controlled Potential on SCC of Nuclear Waste Package Container Materials", *Proceedings of NACE Corrosion 2000*, Paper No. 00188, Orlando, FL (2000)
26. Stress Corrosion Cracking, Metallurgical Consultants Website
(<http://www.materialsengineer.com/CA-scc.htm>)
27. R. J. H. Wanhill, "Aqueous Stress Corrosion in Titanium Alloys", *Br. Corros. J.*, 10, No. 2, pp. 69-78 (1975)
28. G. P. Tiwari, et al., "A study of Internal Hydrogen Embrittlement of Steels", *Materials Science and Engineering*, A286, pp. 269-281 (2000)
29. A. R. Troiano, *Transactions of the American Society of Metals*, 52, pp. 54 (1960)
30. R. A. Oriani, *Annual Review of Materials Science*, 8, pp. 327 (1978)
31. P. Hirth, *Metallurgical Transactions*, 11 A, pp. 861 (1980)
32. Hydrogen Embrittlement, Corrosion Doctors Website
(<http://www.corrosion-doctors.org/Forms/embrittlement.htm>)
33. J. Gu, et al., "Effect of Hydrogen on Structure and Slow Strain Rate Embrittlement of Mill Annealed Ti6Al14V", *Materials Science and Technology*, 12, No. 10, pp. 820-807 (1996)
34. L.C. Covington, "Factors Affecting the Hydrogen Embrittlement of Titanium", *Proceedings of NACE Corrosion 1975*, Toronto, Canada (1975)
35. N.E. Paton, et al., "Effect of Hydrogen on Titanium and its Alloys", *Titanium and Titanium Alloys Source Book*, American Society of Metals, pp. 185-207 (1982)
36. *Metals Handbook, Fractography*, ASM International, 9th Edition, pp. 396 and 453 (1987)

VITA

Graduate College
University of Nevada, Las Vegas

Phani P. Gudipati

Home Address:

1165 Maryland Circle Apt # 3,
Las Vegas, Nevada 89119

Degrees:

Bachelor of Engineering, 2001
University of Mysore, India

Publications:

- Ajit K. Roy, Ramprashad Prabhakaran, Mohammad K. Hossain, Sudheer Sama, Phani P. Gudipati, Venkataramakrishnan Selvaraj, , “Environmental Effects on Materials For Nuclear Applications,” Materials Science & Technology (MS&T) 2003, November 9-12, 2003, Chicago, Illinois
- Ajit K. Roy, ,Ramprashad Prabhakaran, Mohammad K. Hossain, Sudheer Sama, Phani P. Gudipati, Venkataramakrishnan Selvaraj, , “Effect of Environmental Variables on Cracking of Martensitic Stainless Steels under Different Loading Conditions,” American Nuclear Society (ANS) Meeting–Global 2003, Paper No. 87869, November 16-20, 2003, New Orleans, Louisiana
- Ajit K. Roy, Ramprashad Prabhakaran, Mohammad K. Hossain, Sudheer Sama, Phani P. Gudipati ,Venkataramakrishnan Selvaraj, , “Cracking of Target Materials under Cathodic Applied Potential,” The National Association of Corrosion Engineers (NACE)-Corrosion 2004, Paper No. 4559, March 28-April 1, 2004, New Orleans, Louisiana
- Ajit K. Roy, Phani P. Gudipati, Venkataramakrishnan Selvaraj, “ Environment Assisted Cracking in Martensitic Stainless Steels for Transmutation Applications”, Materials Science & Technology (MS&T) 2004, September 27-29, 2004, New Orleans, Louisiana
- Zhiong Wang, Phani P. Gudipati, et al., “Systems Engineering Approach for Optimal Ware House Location Selection”, Las Vegas, Sept 16-18 , 2004

Thesis Title: Stress Corrosion Cracking Resistance of Martensitic Stainless Steels for Transmutation Applications

Thesis Examination Committee:

Chairperson, Dr. Ajit K. Roy, Ph. D.

Committee Member, Dr. Anthony E. Hechanova, Ph. D.

Committee Member, Dr. Brendan J. O'Toole, Ph. D.

Graduate Faculty Representative, Dr. Jacimaria R. Batista, Ph. D.